bioRxiv preprint doi: https://doi.org/10.1101/138701; this version posted January 12, 2018. The copyright holder for this preprint (which was not certified by peer review) is the author/funder. All rights reserved. No reuse allowed without permission.

An FGF-driven feed-forward circuit patterns the cardiopharyngeal mesoderm in space and time

Florian Razy-Krajka, Basile Gravez, Nicole Kaplan, Claudia Racioppi, Wei Wang and Lionel Christiaen*

Center for Developmental Genetics, Department of Biology, College of Arts and Science, New York University, New York, NY, USA

* author for correspondence: email: lc121@nyu.edu, twitter: @lionlchristiaen, phone: +1 212 992 8695

bioRxiv preprint doi: https://doi.org/10.1101/138701; this version posted January 12, 2018. The copyright holder for this preprint (which was not certified by peer review) is the author/funder. All rights reserved. No reuse allowed without permission.

Abstract

In embryos, multipotent progenitors divide to produce distinct progeny and express their full potential. In vertebrates, multipotent cardiopharyngeal progenitors produce second-heart-field-derived cardiomyocytes, and branchiomeric skeletal head muscles. However, the mechanisms underlying these early fate choices remain largely elusive. The tunicate *Ciona* emerged as an attractive model to study early cardiopharyngeal development at high resolution: through two asymmetric and oriented divisions, defined cardiopharyngeal progenitors produce distinct first and second heart precursors, and pharyngeal muscle (aka atrial siphon muscle, ASM) precursors. Here, we demonstrate that differential FGF-MAPK signaling distinguishes between heart and ASM precursors. We characterize a feed-forward circuit that promotes the successive activations of essential ASM determinants, *Hand-related*, *Tbx1/10* and *Ebf*. Finally, we show that coupling FGF-MAPK restriction and cardiopharyngeal network deployment with cell divisions defines the timing of gene expression and permits the emergence of diverse cell types from multipotent progenitors.

bioRxiv preprint doi: https://doi.org/10.1101/138701; this version posted January 12, 2018. The copyright holder for this preprint (which was not certified by peer review) is the author/funder. All rights reserved. No reuse allowed without permission.

Introduction

Developmental genetics knowledge guided progress towards driving mammalian stem cells into forming pure cultures of selected cell types *in vitro* (e.g. (Kattman et al., 2011; Mazzoni et al., 2011; Peljto and Wichterle, 2011). By contrast, in the embryo, pluripotent cells generate diverse cell types in defined proportions, as they divide before individual daughter cells adopt distinct fates.

Subsets of the heart and head/neck myocytes recently emerged as related derivatives of multipotent progenitors located in the cardiopharyngeal mesoderm (Diogo et al., 2015a; Tzahor, 2009; Tzahor and Evans, 2011). Early lineage tracing, transplantations and controlled explant culture experiments demonstrated that the anterior splanchnic/pharyngeal mesoderm of amniote embryos can produce either skeletal muscles or heart tissue, depending upon exposure to growth factors and signaling molecules (Nathan et al., 2008; Tirosh-Finkel et al., 2006; Tzahor et al., 2003; Tzahor and Lassar, 2001). Clonal analyses in the mouse further revealed the existence of common *Mesp1*-expressing progenitors for subsets of the second heart field-derived cardiomyocytes and branchiomeric facial, jaw, neck and even œsophageal muscles (Gopalakrishnan et al., 2015; Lescroart et al., 2014; Lescroart et al., 2015; Lescroart et al., 2010; Lescroart et al., 2012). In pluripotent stem cells, controlled *Mesp1* expression can drive mesodermal progenitors towards cardiac and/or skeletal muscle fates (Bondue et al., 2008; Chan et al., 2016; Chan et al., 2013). Proper development of the pharyngeal apparatus and second heart field derivatives require shared inputs from Tbx1, Nkx2.5 and Islet1 transcription factors (e.g. (Cai et al., 2003; George et al., 2015; Jerome and Papaioannou, 2001; Kelly et al., 2004; Merscher et al., 2001; Mosimann et al., 2015; Nevis et al., 2013; Prall et al., 2007; Tzahor and Evans, 2011; Vitelli et al., 2002a; Watanabe et al., 2012; Witzel et al., 2017; Yagi et al., 2003; Zhang et al., 2006)). Taken together, this growing body of evidence points to the existence of a mesodermal

bioRxiv preprint doi: https://doi.org/10.1101/138701; this version posted January 12, 2018. The copyright holder for this preprint (which was not certified by peer review) is the author/funder. All rights reserved. No reuse allowed without permission.

field of multipotent progenitors capable of producing either SHF-derived cardiomyocytes or branchiomeric skeletal muscles in early vertebrate embryos (Diogo et al., 2015b; Mandal et al., 2017). However, the mechanisms that distinguish fate-restricted heart and head muscle precursors remain largely elusive.

The tunicate Ciona, which is among the closest living relatives to the vertebrates (Delsuc et al., 2006; Putnam et al., 2008), has emerged as a simple chordate model to characterize multipotent cardiopharyngeal progenitors and the mechanisms that initiate heart vs. pharyngeal muscle fate choices (Kaplan et al., 2015; Razy-Krajka et al., 2014; Stolfi et al., 2010; Tolkin and Christiaen, 2016; Wang et al., 2013). Ciona tailbud embryos possess two multipotent cardiopharyngeal progenitors on either side. Like their vertebrate counterparts, these cells emerge from *Mesp+* progenitors towards the end of gastrulation; they are induced by FGF-MAPK signaling and have been termed *trunk ventral cells* (aka TVCs; (Christiaen et al., 2008; Davidson and Levine, 2003; Davidson et al., 2006; Davidson et al., 2005; Satou et al., 2004; Stolfi et al., 2010)). TVCs activate conserved cardiac markers, including *Hand*, *Gata4/5/6* and *Nk4/Nkx2-5*, and migrate as polarized pairs of cells, until the left and right pairs meet at the ventral midline and begin to divide asymmetrically along the mediolateral axis (Figure 1A; (Christiaen et al., 2008; Davidson et al., 2005; Satou et al., 2004; Stolfi et al., 2010)). The first oriented asymmetric divisions produce small median first heart precursors (FHPs), and large lateral second trunk ventral cells (STVCs), which specifically activate *Tbx1/10* (Davidson et al., 2005; Stolfi et al., 2010; Wang et al., 2013). STVCs later divide again to produce small median second heart precursors (SHPs), and large lateral atrial siphon muscle founder cells (ASMFs), which activate *Ebf* (aka *COE*; (Razy-Krajka et al., 2014; Stolfi et al., 2010; Stolfi et al., 2014c)). The transcription factors Hand-related (Hand-r)/Notrlc, which is expressed in the TVCs and maintained in the STVCs and ASMFs after each division, and Tbx1/10 are required for *Ebf* activation in the ASMFs,

bioRxiv preprint doi: https://doi.org/10.1101/138701; this version posted January 12, 2018. The copyright holder for this preprint (which was not certified by peer review) is the author/funder. All rights reserved. No reuse allowed without permission.

whereas Nk4/Nkx2.5 represses *Tbx1/10* and *Ebf* expression in the second heart precursors (SHPs)(Razy-Krajka et al., 2014; Tolkin and Christiaen, 2016; Wang et al., 2013). Conversely, Tbx1/10 and Ebf inhibit cardiac markers, and likely determinants, such as *Gata4/5/6* and *Hand* (Razy-Krajka et al., 2014; Stolfi et al., 2010; Stolfi et al., 2014a; Wang et al., 2013). These regulatory cross-antagonisms underlie the transition from transcriptionally primed multipotent progenitors to separate fate-restricted precursors, by limiting the deployment of the heart- and pharyngeal-muscle-specific programs to their corresponding specific precursors (Kaplan et al., 2015).

Here, we identify regulatory mechanisms ensuring the emergence of diverse fate-restricted precursors from multipotent progenitors. We show that differential FGF-MAPK signaling, feed-forward regulatory circuits and coupling with the cell cycle control the spatially restricted activation of *Tbx1/10* and *Ebf*, successively, thus permitting the emergence of both first and second heart precursors, and ASM/pharyngeal muscle precursors from common multipotent progenitors.

bioRxiv preprint doi: https://doi.org/10.1101/138701; this version posted January 12, 2018. The copyright holder for this preprint (which was not certified by peer review) is the author/funder. All rights reserved. No reuse allowed without permission.

Results

MAPK signaling is active in the multipotent cardiopharyngeal progenitors and progressively restricted to the pharyngeal muscle precursors.

During the earliest stages of cardiopharyngeal development in ascidians, multipotent progenitors display multilineage transcriptional priming, (Razy-Krajka et al., 2014; Stolfi et al., 2014b), and subsequent regulatory cross-antagonisms segregate distinct cardiopharyngeal programs to their corresponding fate-restricted progenitors (Stolfi et al., 2010; Wang et al., 2013); reviewed in (Kaplan et al., 2015)). For instance, the ASM-specific factor Ebf is necessary and sufficient to terminate the heart program and impose a pharyngeal muscle fate (Razy-Krajka et al., 2014; Stolfi et al., 2010). However, the symmetry-breaking events leading to cardiopharyngeal mesoderm patterning and ASM-specific expression of *Ebf* remain unknown. We surmised that differential signaling inputs determine the stereotyped spatio-temporal patterning of early cardiopharyngeal progenitors.

The Ciona homologs of specific FGF-MAPK pathway components, including *FGF receptor substrate 2/3* (*Frs2/3*; (Gotoh et al., 2004)), *Ets.b*, and *Fgf4/5/6*, are preferentially expressed in the TVCs, in the STVCs and in the ASMFs as cells transition from multipotent progenitor to distinct heart vs. ASM fate-restricted states (Razy-Krajka et al., 2014). These patterned expressions of MAPK effector genes prompted us to evaluate a role for FGF-MAPK pathway in cardiopharyngeal fate decisions.

We first used an antibody specific to the dual phosphorylated form of Extracellular Regulated Kinase (dpERK) to monitor Mitogen Activated Protein Kinase (MAPK) activity in the cardiopharyngeal mesoderm. We detected dpERK staining in the newly born TVCs, marked by the B7.5-lineage-specific *Mesp>H2B::mCherry* transgene (Figure S1), as previously observed (Davidson et al, 2006). We also detected weaker but

bioRxiv preprint doi: https://doi.org/10.1101/138701; this version posted January 12, 2018. The copyright holder for this preprint (which was not certified by peer review) is the author/funder. All rights reserved. No reuse allowed without permission.

persistent dpERK staining in the TVCs during migration (Figures 1 and S1). Following the first and second asymmetric divisions of the TVCs and STVCs, dpERK staining was successively restricted to the more lateral STVCs and ASMFs, respectively (Figures 1A, B; S1).

The canonical FGF/Ras/MEK/ERK pathway is necessary and sufficient to promote pharyngeal muscle specification in the cardiopharyngeal lineage.

This exclusion of MAPK activity from the medial first and second heart precursors opened the possibility that differential ERK activity is required for proper STVC and ASMF vs. heart precursors fate decisions. In Ciona, signaling through the sole FGF receptor (FGFR) governs ERK activity in several developmental processes, including neural induction (Bertrand et al., 2003; Hudson et al., 2003) and central nervous system patterning (Haupaix et al., 2014; Racioppi et al., 2014; Stolfi et al., 2011; Wagner et al., 2014), early endomesoderm and notochord fate specification (Imai et al., 2002; Picco et al., 2007; Shi and Levine, 2008; Shi et al., 2009; Yasuo and Hudson, 2007). Notably, FGF-MAPK signaling is active in the *Mesp*+ cardiogenic B7.5 blastomeres (Imai et al., 2006; Shi and Levine, 2008), where targeted misexpression of a dominant negative form of FGFR (dnFGFR) blocks TVC induction (Christiaen et al., 2008; Davidson et al., 2006). We used a TVC-specific *Foxf* enhancer (*Foxf(TVC):bpFog-1>dnFGFR::mCherry*, hereafter called *Foxf>dnFGFR*; (Beh et al., 2007)), to bypass early effects and achieve later misexpression of dnFGFR in the TVCs and their progeny. Importantly, although TVC fate specification and the onset of *Foxf* expression require FGF-MAPK signaling (Beh et al., 2007; Davidson et al., 2006), we confirmed that this perturbation altered neither initial TVC induction, nor the expression of the *Foxf* driver (Figure S2). Consistent with proper TVC induction, *Foxf>dnFGFR* prevented neither TVC migration nor asymmetric divisions, but it abolished the expression of both

bioRxiv preprint doi: https://doi.org/10.1101/138701; this version posted January 12, 2018. The copyright holder for this preprint (which was not certified by peer review) is the author/funder. All rights reserved. No reuse allowed without permission.

147 *Tbx1/10* in the STVCs and *Ebf* in the ASMFs (Figure 1C). This data indicate that FGF-
148 MAPK signaling is required in the cardiopharyngeal progenitors and/or their progeny
149 for ASM fate specification, beyond the initial TVC induction.

150 Upon FGF-MAPK-dependent induction, the TVCs express *Hand-related/Hand-r*
151 (renamed after *Notrlc/Hand-like*; (Christiaen et al., 2008; Davidson and Levine, 2003;
152 Davidson et al., 2006; Satou et al., 2004; Stolfi et al., 2014c; Woznica et al., 2012)),
153 which encodes a basic helix-loop-helix (bHLH) transcription factor necessary for *Ebf*
154 expression in the ASMFs (Razy-Krajka et al, 2014). Moreover, the *Hand-r* TVC
155 enhancer contains putative Ets1/2 binding sites, which are necessary for reporter gene
156 expression, and presumably mediate the transcriptional inputs of FGF-MAPK (Woznica
157 et al., 2012). Since *Hand-r* and *Foxf* expressions start at approximately the same time in
158 newborn TVCs, we used *Foxf>dnFGFR*, which did not alter the onset of *Hand-r*
159 expression in the TVCs (Figure S2), to test whether the maintenance of *Hand-r*
160 expression in migratory TVCs requires prolonged FGF-MAPK inputs. *Foxf>dnFGFR*
161 inhibited *Hand*-r expression in late TVCs (Figure 1C), indicating that sustained *Hand-r*
162 expression requires continuous FGF-MAPK signaling, as did TVC-expressed FGF-
163 MAPK pathway components (Figure S2).

164 To test whether the spatial restriction of MAPK activity explains the patterned
165 expressions of *Hand-r*, *Tbx1/10* and *Ebf* following asymmetric cell divisions, we used
166 gain-of-function perturbations to force FGF-MAPK activity throughout the
167 cardiopharyngeal mesoderm and assayed gene expression (Figure 2). We focused on the
168 canonical FGF-MAPK pathway where signal transduction involves Ras, Raf, MEK and
169 ERK downstream of FGFR and upstream of transcriptional effectors (Lemmon and
170 Schlessinger, 2010). We first used M-Ras^{G22V}, a defined constitutively active form of M-
171 Ras, which mediates FGF signaling in *Ciona*, where other classical *Ras* genes are
172 missing (Keduka et al., 2009), and focused on *Htr7* and *Tbx1/10* expression following

bioRxiv preprint doi: https://doi.org/10.1101/138701; this version posted January 12, 2018. The copyright holder for this preprint (which was not certified by peer review) is the author/funder. All rights reserved. No reuse allowed without permission.

the first asymmetric TVC division in 15 hours post-fertilization (hpf) embryos. *Htr7* encodes a *trans*-membrane G-protein coupled receptor and, like *Hand-r*, its expression and maintenance in the TVCs require MAPK activity (Figure S2; (Razy-Krajka et al., 2014)), and become restricted to the lateral STVC following asymmetric division. However, *Htr7* mRNAs are cleared more rapidly from the FHPs, making the patterned expression easier to analyze than that of *Hand-r* (Figures 2 and 3D; (Razy-Krajka et al., 2014)). Importantly, misexpression of M-Ras^{G22V} using the TVC-specific *Foxf* enhancer altered cell division asymmetry and/or orientation in under 50% of the embryos, still allowing us to identify large lateral and small median cells in a small majority of embryos (Figure S3). Compared to control embryos overexpressing wild-type M-Ras (M-Ras^{WT}), TVC-specific gain of M-Ras function caused both persistent *Htr7* expression and ectopic activation of *Tbx1/10* in the small median cells following asymmetric divisions (Figure 2B,C). Similarly, *Foxf>M-Ras^{G22V}*-expressing 18hpf larvae displayed ectopic *Ebf* activation throughout the cardiopharyngeal mesoderm (Figure 2B,C). This cannot be simply accounted for by general disruption of cell division patterns at this later stage (Figure S3), since similar disruptions can be caused by *Foxf>dnFGFR*, which inhibits *Ebf* expression (Figure 1C). These results indicated that forced M-Ras activity is sufficient to upregulate STVC and ASMF markers ectopically. This is consistent with the idea that spatially defined signaling upstream of M-Ras restricts MAPK activity, thus localizing STVC- and ASM-specific gene activities.

To further probe the signal transduction pathway, we engineered a constitutively active version of the Ciona Mek1/2 protein by introducing phosphomimetic mutations of two conserved serine residues in the catalytic domain, as previously shown for the mammalian homolog (Cowley et al., 1994; Mansour et al., 1994). Early misexpression of Mek^{S220E,S216D} in the B7.5 lineage using the *Mesp* enhancer caused ectopic TVC induction, mimicking the effects of gain of Ets1/2 function (Figure S4; (Davidson et al.,

bioRxiv preprint doi: https://doi.org/10.1101/138701; this version posted January 12, 2018. The copyright holder for this preprint (which was not certified by peer review) is the author/funder. All rights reserved. No reuse allowed without permission.

2006)). As seen with M-Ras^{G22V}, TVC-specific misexpression of Mek^{S220E,S216D} using the *Foxf* enhancer also caused ectopic expression of *Htr7* and *Tbx1/10*, and *Ebf* in 15 and 18hpf larvae, respectively (Figure 2B, C). Taken together, these results indicate that activity of the canonical FGF-Ras-MEK-ERK pathway is progressively restricted to the STVC and ASMF, and is both necessary and sufficient to promote STVC- and ASMF-specific gene expressions.

Continuous FGF-MAPK activity is required for the successive activations of *Tbx1/10* and *Ebf*.

FGF-MAPK signaling is sufficient and necessary to maintain *Hand-r* expression in late TVCs (Figure 1), and *Hand-r* is necessary for *Ebf* expression in the ASMF (Razy-Krajka et al., 2014). Therefore, it is possible that later FGF-MAPK signaling is dispensable for *Tbx1/10* and *Ebf* activation and ASM specification, as long as STVC and ASMF cells inherit sustained levels of *Hand-r* mRNAs and/or proteins. To disentangle late from early requirements of FGF-MAPK signaling, we incubated embryos at different stages with the MEK/MAPKK inhibitor U0126, which abolishes dual ERK phosphorylation and the initial MAPK-dependent TVC induction in Ciona embryos (Figure S1; (Davidson et al., 2006; Hudson et al., 2003)). MEK inhibition during TVC migration (i.e. between 9.5 and 12.5 hpf, Figure 3A) blocked the expression of *Hand-r* and *Htr7* in late TVCs (Figure 3B, E). U0126 treatments in late TVCs, and through the first asymmetric division (i.e. between 12 and 15 hpf, Figure 3A) did not alter TVC division patterns (Figure S3C), but it blocked both the maintenance of *Hand-r* and *Htr7*, and the activation of *Tbx1/10* in the STVCs (Figure 3C, D, F, G). Finally, MEK inhibition in late STVCs and through asymmetric divisions (i.e. between 15 and 18 hpf) also did not alter STVC divisions (Figure S3G), but it blocked the ASMF-specific expression of *Ebf* (Figure 3H). These results indicate that continuous MEK activity is

bioRxiv preprint doi: https://doi.org/10.1101/138701; this version posted January 12, 2018. The copyright holder for this preprint (which was not certified by peer review) is the author/funder. All rights reserved. No reuse allowed without permission.

required throughout cardiopharyngeal development to successively activate TVC-, STVC-, and ASMF-expressed genes.

Since *Ebf* expression is maintained for several days in the ASMF derivatives as they differentiate into body wall and siphon muscles (Razy-Krajka et al., 2014), we tested whether continued MEK activity is also required for the maintenance of *Ebf* expression past its onset and cells' commitment to an ASM fate. Using both regular and intron-specific antisense probes, which specifically detect nascent transcripts (Wang et al., 2013), we showed that later MEK inhibition (i.e. U0126 incubation between 17 and 20 hpf) did not block the maintenance of *Ebf* transcription in the ASMPs (Figure 3I, J). This indicates that sustained MEK activity is required until the onset of *Ebf* expression, but not beyond, and the maintenance of *Ebf* expression during ASM development is independent of MAPK.

Since U0126 treatments affect the whole embryo, we sought to further confirm the later roles for FGF-MAPK signaling specifically in the cardiopharyngeal mesoderm. To this aim, we used an STVC-specific enhancer from the *Tbx1/10* locus (termed *T6*; Figure 3K, L; Figure S5; (Tolkin and Christiaen, 2016); Racioppi et al., in preparation) to drive expression of either dnFGFR or the constitutively active M-Ras^{G22V} starting at ~14hpf, and assayed *Ebf* expression at 18hpf (Figure 3K, L). These perturbations minimally affected the cell division patterns (Figure S3), such that cells corresponding to FHP, SHP and ASMF could be identified by their position relative to the midline in many embryos (Figure 3K). M-Ras^{G22V} misexpression caused conspicuous ectopic *Ebf* expression in the SHPs, whereas dnFGFR-mediated inhibition of MAPK activity blocked *Ebf* activation in the lateral ASMFs. These results support the notion that localized FGF-MAPK activity is necessary and sufficient for ASMF-specific expression of *Ebf*.

bioRxiv preprint doi: https://doi.org/10.1101/138701; this version posted January 12, 2018. The copyright holder for this preprint (which was not certified by peer review) is the author/funder. All rights reserved. No reuse allowed without permission.

Coherent feed-forward circuits for cardiopharyngeal mesoderm patterning and ASM fate specification.

The above results indicate that *Hand-r*, *Tbx1/10* and *Ebf* require ongoing FGF-MAPK activity for their successive activations in the TVCs, STVCs and ASMFs, respectively. We previously showed that RNAi and/or CRISPR-mediated inhibition of either *Hand-r* or *Tbx1/10* function blocks *Ebf* activation in the ASMFs, where both *Hand-r* and *Tbx1/10* expressions are maintained (Razy-Krajka et al., 2014; Tolkin and Christiaen, 2016; Wang et al., 2013). We used epistasis assays to systematically test whether early regulators mediate the effects of FGF-MAPK on later gene expression and ASM fate specification, or whether FGF-MAPK signaling acts both upstream and in parallel to early regulators in a more complex regulatory circuit.

We first revisited the regulatory relationships between FGF-MAPK, *Hand-r* and *Tbx1/10* in late TVCs and early STVCs. We validated single guide RNAs (sgRNAs) for CRISPR/Cas9-mediated mutagenesis of *Hand-r* (Table S1; (Gandhi et al., 2017a)), and determined that *Hand-r* function is necessary for *Tbx1/10* activation in the STVCs (Figure 4A). Co-expression of a CRISPR-resistant *Hand-r* cDNA (Hand-r^{PAMmis}) rescued *Tbx1/10* expression in the STVCs, indicating that *Tbx1/10* down-regulation in this CRISPR "background" is specifically due to *Hand-r* loss-of-function (Figure 4A). To further probe if *Hand-r* activity is necessary for FGF-MAPK-dependent *Tbx1/10* expression, we used gain of M-Ras function in a *Hand-r* CRISPR "background". Whereas, misexpression of the constitutively active M-Ras^{G22V} caused ectopic *Tbx1/10* expression, concomitant loss of *Hand-r* function diminished both endogenous and ectopic *Tbx1/10* expression in the STVC and FHP, respectively (Figure 4A). Although, remaining ectopic activation could still be observed, possibly because M-Ras^{G22V} could boost *Hand-r* expression in heterozygous cells where CRISPR/Cas9 disrupted only one

bioRxiv preprint doi: https://doi.org/10.1101/138701; this version posted January 12, 2018. The copyright holder for this preprint (which was not certified by peer review) is the author/funder. All rights reserved. No reuse allowed without permission.

276 copy of the gene. This data indicate that Hand-r function is necessary for FGF-MAPK-
277 induced activation of *Tbx1/10*.

278 To further probe the epistatic relationships between *Hand-r* and MAPK signaling
279 upstream of *Tbx1/10*, we attempted to rescue *Tbx1/10* expression in U0126-treated
280 embryos, by over-expressing *Hand-r* with the TVC-specific *Foxf* enhancer. Neither did
281 Hand-r over-expression cause ectopic *Tbx1/10* activation (in the FHPs), nor was it
282 sufficient to rescue *Tbx1/10* expression in 15hpf STVCs (Figure 4B). Taken together,
283 these data indicate that both Hand-r and MAPK activities are required to activate
284 *Tbx1/10* in the STVCs. These results also imply that MAPK signaling is restricted to the
285 STVC independently of Hand-r activity, which suffice to explain the STVC-specific
286 activation of *Tbx1/10*. Finally, we isolated a minimal STVC-specific enhancer from the
287 *Tbx1/10* locus and identified conserved putative Ets binding sites, which were necessary
288 for reporter gene expression (Figure S5). This suggests that the FGF-MAPK-Ets
289 pathway directly regulates *Tbx1/10* expression in the STVCs.
290
291 Next, we investigated the epistatic relationship between FGF-MAPK, *Hand-r*, and
292 *Tbx1/10* upstream of *Ebf* in the ASMFs. We first used previously validated
293 CRIPSR/Cas9 reagents targeting the *Tbx1/10* coding region (Tolkin and Christiaen,
294 2016), to confirm that B7.5-lineage-specific loss of *Tbx1/10* function inhibited *Ebf*
295 activation, and verified that this effect could be rescued by over-expression of a
296 CRISPR/Cas9-resistant *Tbx1/10* cDNA, expressed with a minimal TVC-specific *Foxf*
297 enhancer (Figure 4C; Tbx1/10^{PAMmis}). In these rescue experiments, we observed ectopic
298 *Ebf* activation in the SHP, as previously described when driving Tbx1/10 expression
299 with a TVC-specific *Foxf* enhancer (Wang et al., 2013). As explained below, this ectopic
300 activation could be attributed to a precocious expression of *Ebf* in the STVCs (Figure
301 4E). To test whether *Tbx1/10* was also required for ectopic *Ebf* expression in response to

bioRxiv preprint doi: https://doi.org/10.1101/138701; this version posted January 12, 2018. The copyright holder for this preprint (which was not certified by peer review) is the author/funder. All rights reserved. No reuse allowed without permission.

MAPK activation (see Figure 2), we combined CRISPR/Cas9-mediated *Tbx1/10* knockout with constitutive MAPK activation using the M-Ras^{G22V} mutant and observed a significant inhibition of both endogenous and ectopic *Ebf* expression in the 18hpf ASMF and SHP, respectively (Figure 4C). Taken together, these results show that *Tbx1/10* function is necessary for FGF-MAPK-induced expression of *Ebf* in the ASMFs.

To further test whether *Tbx1/10* acts in parallel and/or downstream of MAPK to activate *Ebf*, we combined gain of *Tbx1/10* function with perturbations of FGF-MAPK signaling and assayed *Ebf* expression. We realized that *Foxf*-driven misexpression of Tbx1/10 caused precocious *Ebf* activation in 15hpf STVCs (Figure 4D, E). This precocious expression remained remarkably patterned, suggesting that STVC-restricted FGF-MAPK activity prevented *Ebf* expression in the dpERK-negative, small median FHPs (Figures 1B, 4E, S1). Indeed, co-expression of Tbx1/10 and M-Ras^{G22V} caused both precocious and ectopic *Ebf* expression in the 15hpf medial and lateral TVC derivatives, which would be FHPs and STVCs in control embryos, respectively. This data confirms that Tbx1/10 misexpression does not suffice to cause ectopic *Ebf* expression in the FHPs, because the latter presumably lack FGF-MAPK activity, as is the case in control embryos.

U0126-mediated MEK inhibition from 12 to 15hpf, i.e. after the onset of *Foxf>Tbx1/10* misexpression, further confirmed that MAPK activity is required in parallel to Tbx1/10 for precocious *Ebf* activation in 15hpf STVCs (Figure 4D, E). Taken together, these results indicate that Tbx1/10 and MAPK are both required to activate *Ebf* in the cell cycle following that of *Tbx1/10* onset.

Since *Hand-r* expression is maintained in the ASMF, and CRISPR/Cas9- or RNAi-mediated *Hand-r* knockdown blocked both *Tbx1/10* (Figure 4A) and *Ebf* expression (Razy-Krajka et al., 2014), we reasoned that Hand-r could also act both upstream and in

bioRxiv preprint doi: https://doi.org/10.1101/138701; this version posted January 12, 2018. The copyright holder for this preprint (which was not certified by peer review) is the author/funder. All rights reserved. No reuse allowed without permission.

parallel to Tbx1/10 for *Ebf* activation. To test this possibility, we assayed *Ebf* expression in 18hpf ASMF following defined perturbations of Hand-r and Tbx1/10. As expected, CRISPR/Cas9-mediated *Hand-r* mutagenesis strongly inhibited *Ebf* expression, and this effect could be rescued by a CRISPR-resistant *Hand-r* cDNA (Figure 4F). To test whether this effect was mediated by a loss of *Tbx1/10* expression, we attempted to rescue the Hand-r loss-of-function by over-expressing Tbx1/10 using the *Foxf* enhancer. As explained above, *Foxf*-mediated Tbx1/10 misexpression caused precocious and ectopic *Ebf* expression in larvae co-electroporated with control sgRNAs (Figure 4D, E, F). By contrast, combining loss of Hand-r function with Tbx1/10 misexpression inhibited both the endogenous and ectopic *Ebf* expression (Figure 4F), indicating that Hand-r is also required in parallel to Tbx1/10 for *Ebf* activation in the ASMFs.

Taken together, these analyses suggest that coherent feed-forward circuits govern the sequential activation of *Hand-r*, *Tbx1/10* and *Ebf* in response to continuous but progressively restricted FGF-MAPK inputs (Figure 4G), thus linking spatial patterning to the temporal deployment of the regulatory cascade leading to localized *Ebf* activation and pharyngeal muscle specification.

The cell cycle entrains the temporal deployment of the cardiopharyngeal gene regulatory network.

In principle, the feed-forward circuit described above is sufficient to explain the successive activations of *Hand-r*, *Tbx1/10* and *Ebf*. However, *Tbx1/10* and *Ebf* do not turn on until after TVC and STVC divisions, respectively. Notably, even when we misexpressed Tbx1/10 in the TVCs, *Ebf* was activated only after cell division and in the lateral-most cells, where FGF-MAPK signaling is normally maintained (Figures 1B, 4E). This sequence of events -divisions followed by gene activation- is paramount as it permits the birth of first and second heart precursors, whose fates are antagonized by

bioRxiv preprint doi: https://doi.org/10.1101/138701; this version posted January 12, 2018. The copyright holder for this preprint (which was not certified by peer review) is the author/funder. All rights reserved. No reuse allowed without permission.

Tbx1/10 and Ebf (Razy-Krajka et al., 2014; Stolfi et al., 2010; Wang et al., 2013). Therefore, we sought to investigate the role(s) of the cell cycle in controlling the timing of *Tbx1/10* and *Ebf* activation.

We first evaluated the effects of cytochalasin B, a classic inhibitor of cytokinesis widely used to study cell fate specification in ascidians (Figure 5A; (Whittaker, 1973)). Treatments starting before TVC divisions (12 hpf) did not block *Tbx1/10* or *Ebf* expression in embryos fixed after their normal onset at either 16 or 19hpf, respectively (Figure 5B). Similarly, treatment starting between the first and second asymmetric divisions (15hpf) did not block localized *Ebf* expression at 19hpf (Figure 5B). This indicates that *Tbx1/10* and *Ebf* activations occur by default in the absence of cytokinesis, most likely because FGF-MAPK signaling persists throughout the shared cytoplasm. This data thus illustrates how the spatial restriction of FGF-MAPK signaling, following cell divisions, leads to the localized activations of *Tbx1/10* and *Ebf*.

Cytochalasin treatments usually lead to the formation of polynucleated cells (e.g. Figure 5B, middle panel), because the cell cycle and nucleokinesis continue. To alter cell cycle progression more comprehensively, and specifically in the cardiopharyngeal lineage, we used genetically encoded inhibitors of cell cycle transitions: Cdkn1b.a and Cdkn1b.b (also known as Noto16), the ortholog of which is a potent inhibitor of the G1/S transition in the ascidian species *Halocynthia roretzi* (Kuwajima et al., 2014), and the G2/M inhibitor Wee1 (Dumollard et al., 2017). We used the TVC-specific *Foxf* enhancer to misexpress these negative regulators of cell cycle progression, monitored cell divisions and assayed *Tbx1/10* expression at 15hpf, when control TVCs have divided and the lateral-most STVCs normally express *Tbx1/10*. Each perturbation efficiently inhibited TVC divisions, such that only two cells were visible on either side of the embryos (Figure 5D). In these delayed TVCs, *Tbx1/10* expression was strongly reduced compared to control STVCs (Figure 5D). However, 20 to 40% of the delayed TVCs

bioRxiv preprint doi: https://doi.org/10.1101/138701; this version posted January 12, 2018. The copyright holder for this preprint (which was not certified by peer review) is the author/funder. All rights reserved. No reuse allowed without permission.

expressed *Tbx1/10* to variable extents. This suggests that the cardiopharyngeal regulatory network can qualitatively unfold independently of cell cycle progression, but the latter is necessary for *Tbx1/10* expression to its wild-type levels.

We next used the STVC-specific *Tbx1/10 T6* enhancer (Figure S5), to misexpress Cdkn1b.a, Noto16 and Wee1, and assayed *Ebf* expression at later stages. Inhibitors of the G1/S transition failed to block STVC divisions (data not shown), most likely because *Tbx1/10(T6)*-driven products did not accumulate quickly enough to interfere with the G1/S transition in STVCs, since this cell cycle lasts only ~2 hours compared to ~6 hours for the TVC interphase. Therefore, we focused the analyses of *Ebf* response to cell cycle perturbations on misexpression of the G2/M inhibitor Wee1. Analyses of 18hpf larvae, fixed approximately 2 hours after the documented onset of *Ebf* expression in ASMFs (Razy-Krajka et al., 2014), indicated that *Ebf* can turn on in arrested STVCs that failed to divide upon Wee1 misexpression (Figure 5E).

Because ~30% of the embryos showed variable expression, as was the case for *Tbx1/10* in the previous experiment, we reasoned that perturbations of the G2/M transition could alter the dynamics of *Ebf* upregulation. We investigated this possibility using embryos fixed every 30 minutes between 15.5hpf and 18hpf, when cells transition from a late *Tbx1/10*+; *Ebf*- STVC state to a committed *Ebf*+, *Mrf*+ ASMF state (Razy-Krajka et al., 2014; Wang et al., 2013). First, we scored the proportion of embryos with delayed STVCs or conspicuous ASMFs at each time point and showed that Wee1 misexpression strongly delays cell cycle progression, blocking cell divisions in a substantial fraction of embryos (Figure S6).

The proportion of *Ebf*+ ASMFs in control embryos progressively increased from ~20% at 15.5hpf to >90% by 18hpf, revealing an under-appreciated dynamic at the onset of *Ebf* expression, which appears to take at least one hour to be "strongly" expressed in >75% of newborn ASMFs (Figure S6).

bioRxiv preprint doi: https://doi.org/10.1101/138701; this version posted January 12, 2018. The copyright holder for this preprint (which was not certified by peer review) is the author/funder. All rights reserved. No reuse allowed without permission.

To evaluate the impact of Wee1-induced mitosis inhibition on *Ebf* accumulation, we focused on undivided STVCs at each time point (hence the lower numbers in Figure S6A compare to Figure S6B). By 17hpf, wee1-expressing delayed STVCs showed "strong" *Ebf* expression in comparably high proportions of embryos. However, these proportions were significantly lower at 16 and 16.5hpf (Chi-square tests, P=0.002 and P=0.0003, respectively), with ~1.5 and ~1.2 times less "strongly" expressing cells than in the control distributions (hypergeometric tests, P=0.0005 and P=0.0001, respectively). These semi-quantitative analyses suggest that the cardiopharyngeal network can eventually unfold independently of cell divisions, leading to high levels of *Ebf* expression, albeit with a delay. This suggests that STVC division entrains *Ebf* upregulation in early ASMFs.

Finally, we reasoned that Wee1-expressed delayed STVC that activate *Ebf* would not turn on heart markers (Wang et al., 2017). Indeed, delayed STVCs failed to activate the pan-cardiac *Lrp4/8*, and the SHP-markers *Kirr* and *Dach* (Figure 5F; (Wang et al., 2017). This indicated that coupling STVC division with localized FGF-MAPK activity and timed *Ebf* upregulation permits the localized activation of *Ebf* and the emergence of cardiac progenitors.

Transition from a MAPK-dependent to a MAPK-independent and autoregulative mode of *Ebf* expression in early ASMFs.

We sought to further probe the mechanisms that regulate the initiation of *Ebf* expression in early ASMFs, and their biological significance for fate specification. Since we observed a progressive accumulation of *Ebf* mRNAs, and a transition from a MAPK-dependent onset to a MAPK-independent maintenance of *Ebf* transcription (Figure 3I, J), we reasoned that the window of MAPK-dependence might coincide with the accumulation of *Ebf* mRNAs between 16 and 17hpf. To test this possibility, we treated

bioRxiv preprint doi: https://doi.org/10.1101/138701; this version posted January 12, 2018. The copyright holder for this preprint (which was not certified by peer review) is the author/funder. All rights reserved. No reuse allowed without permission.

embryos with the MEK inhibitor U0126 at successive time points, assayed ongoing transcription using intronic probes and counted the numbers of *Ebf* transcribing cells (Figure 6A). This analysis revealed that *Ebf* transcription gradually lost its sensitivity to MAPK inhibition between 16 and 17hpf, i.e. during the first hour of the ASMF cycle when *Ebf* mRNAs normally accumulate (Figure S6A,B).

Because *Ebf* transcription becomes independent from MAPK by the time *Ebf* mRNA have accumulated to "high" levels, and because *Ebf* expression lasts for several days in the progeny of the ASMFs, we reasoned that autoregulation might suffice to maintain high levels of *Ebf* mRNA past the MAPK-dependent onset. To test this possibility, we misexpressed the Ebf coding sequence using the STVC-specific *T6* enhancer as described (Tolkin and Christiaen, 2016). Assaying endogenous *Ebf* transcription with intronic probes demonstrated that, in addition to its normal expression in the ASMFs, Ebf misexpression caused precocious and ectopic activation of the endogenous locus in the STVCs, and in the MAPK-negative SHPs, respectively (Figure 6C-F). This result suggests that *Ebf* transcription bypasses both requirements for cell-division coupling and MAPK inputs if high levels of *Ebf* gene products are present in the cell.

We reasoned that, if high levels of *Ebf* expression can promote its own transcription independently of MAPK signaling, then Ebf misexpression should be sufficient to rescue a chemical inhibition of MAPK at a critical stage. We tested this possibility by combining Ebf misexpression using the STVC-specific *T6* enhancer and U0126 treatments starting at 16hpf, which normally block *Ebf* expression (Figure 6A, D-F). We observed that transcription of the endogenous *Ebf* locus became independent of early MAPK activity upon misexpression of an Ebf cDNA, further supporting the notion that high levels of *Ebf* expression suffice to maintain *Ebf* transcription independently of MAPK activity.

bioRxiv preprint doi: https://doi.org/10.1101/138701; this version posted January 12, 2018. The copyright holder for this preprint (which was not certified by peer review) is the author/funder. All rights reserved. No reuse allowed without permission.

458 A potentially important implication of this transient MAPK requirement is to render
459 *Ebf* expression initially reversible. For instance, *Ebf* occasionally turns on precociously
460 in the STVCs of a small proportion of embryos (Figure S6C). Given the powerful anti-
461 cardiogenic effects of Ebf (Razy-Krajka et al., 2014; Stolfi et al., 2010), persistent *Ebf*
462 expression would have dramatic consequences for SHP development (Wang et al.,
463 2013). However, because MAPK activity is excluded from the SHPs, and the early phase
464 of *Ebf* expression depends upon continuous MAPK activity, we surmise that *Ebf* cannot
465 be maintained in the SHPs. For instance, when embryos from the same electroporated
466 batch were fixed at the time of early U0126 treatment (i.e. 15.75 and 16.25hpf) and ~4
467 hours later, at 20hpf, and assayed for *Ebf* transcription using intronic probes, initially
468 wild-type patterns of *Ebf* transcription could not be maintained (Figure S7A). This
469 suggests that, although *Ebf* can be activated precociously in a MAPK-dependent
470 manner, its expression shuts off in the SHPs upon MAPK inhibition following STVC
471 division.

472 We further addressed the interplay between cell division, MAPK signaling and *Ebf*
473 expression. We reasoned that, if cell divisions entrain Ebf accumulation and the
474 transition to a MAPK-independent autoregulative mode, then delaying STVC divisions
475 should extend the period of MAPK-dependent *Ebf* transcription. We tested this
476 possibility by expressing Wee1 under the control of the STVC-specific *T6* enhancer, and
477 treated embryos with U0126 at 17hpf, which inhibited the maintenance of *Ebf*
478 transcription in only 15% to 20% of the control embryos (Figures 6A, S7B). The
479 proportion of embryos showing U0126-sensitive *Ebf* transcription increased to almost
480 50% upon *T12>Wee1* expression (Figure S7B), which is consistent with our hypothesis
481 that inhibiting the G2/M transition delays the accumulation of *Ebf* gene products, thus
482 postponing the transition from a low level/MAPK-dependent to an high level/MAPK-
483 independent and self-activating mode of *Ebf* regulation.

bioRxiv preprint doi: https://doi.org/10.1101/138701; this version posted January 12, 2018. The copyright holder for this preprint (which was not certified by peer review) is the author/funder. All rights reserved. No reuse allowed without permission.

We propose a model for *Ebf* regulation whereby Hand-r, Tbx1/10, ongoing MAPK signaling and cell-cycle-regulated transcriptional input(s) govern the onset and initial accumulation of *Ebf* gene products during the first hour of the ASMF cycle, whereas the maintenance of *Ebf* expression relies primarily on MAPK-independent autoactivation, following initial accumulation (Figure 7).

bioRxiv preprint doi: https://doi.org/10.1101/138701; this version posted January 12, 2018. The copyright holder for this preprint (which was not certified by peer review) is the author/funder. All rights reserved. No reuse allowed without permission.

Discussion

Here, we demonstrated that the progressive restriction of FGF-MAPK signaling follows oriented and asymmetric cell divisions of multipotent progenitors and patterns the ascidian cardiopharyngeal mesoderm in space and time. Dynamic FGF-MAPK activity patterns lead to the localized expression of *Hand-r*, *Tbx1/10* and *Ebf* in fate-restricted pharyngeal muscle precursors, and their concomitant exclusion for first and second heart precursors. We show that coherent feedforward circuits encode the successive activations of *Hand-r*, *Tbx1/10* and *Ebf*, whereas cell divisions entrain the progression of this regulatory sequence and thus define the timing of gene expression. Finally, we provide evidence that the initiation of *Ebf* expression depends on MAPK activity in early ASMF, until Ebf accumulation permits MAPK-independent auto-activation. Given the potent anti-cardiogenic, and pro-pharyngeal muscle effects of Ebf (Razy-Krajka et al., 2014; Stolfi et al., 2010), we surmise that the latter switch corresponds to the transition from a cardiopharyngeal multipotent state to a committed pharyngeal muscle identity.

Spatial patterning by localized maintenance of FGF-MAPK signaling.

Our results demonstrate that MAPK signaling is maintained only in the lateral-most daughter cells following each asymmetric division of multipotent cardiopharyngeal progenitors - the TVCs and STVCs. This asymmetric maintenance is necessary and sufficient for the progressive and localized deployment of the pharyngeal muscle network. Notably, the TVCs themselves are initially induced by similar polarized FGF-MAPK signaling coincidental to asymmetric cell divisions of their mother cells, the B8.9 and B8.10 founder cells (Davidson et al., 2006). At this stage, asymmetrical maintenance of sustained FGF-MAPK signaling involves intrinsic Cdc42-dependent polarity of the founder cells, which promotes polarized cell-matrix adhesion of the

bioRxiv preprint doi: https://doi.org/10.1101/138701; this version posted January 12, 2018. The copyright holder for this preprint (which was not certified by peer review) is the author/funder. All rights reserved. No reuse allowed without permission.

prospective TVC membrane to the ventral epidermis. The latter differential integrin-mediated adhesion promotes localized MAPK activation, leading to TVC induction (Cooley et al., 2011; Norton et al., 2013). It has been proposed that adhesion- and caveolin-dependent polarized FGFR recycling during mitosis accounts for the localized activation of MAPK in the prospective TVCs (Cota and Davidson, 2015). Whereas similar mechanisms could in principle account for asymmetric maintenance of FGF-MAPK signaling in STVCs and ASMFs, this has not been formally tested and there are notable differences opening the possibility that other mechanisms may be at work: during TVC induction, MAPK signaling is maintained in the smaller daughter cell that contacts the epidermis, whereas in the following divisions, MAPK activity persists in the larger daughter cells and all cells maintain contact with the epidermis (Kaplan et al., in preparation). Moreover, using fusion proteins as in previous studies, we could not observed a marked polarized distribution of FGFR molecules to the lateral-most cells (the STVCs and ASMFs; Kaplan et al., in preparation). However, the fact that constitutively active forms of M-Ras and Mek1/2 were sufficient to bypass the loss of MAPK activity, and impose pharyngeal muscle specification, indicates that differential FGF-MAPK activity is regulated upstream of M-Ras. Further work is needed to elucidate the cellular and molecular mechanisms governing the spatiotemporal patterns of FGF-MAPK signaling in the cardiopharyngeal mesoderm. In particular, it will be important to disentangle the relative impacts of extrinsic (i.e. tissues, contacts) vs. intrinsic (i.e. asymmetric cell division) effects onto FGF-MAPK signaling and the downstream transcriptional inputs.

Our preliminary analyses indicate that perturbations of the FGF-Ras-MEK pathway can alter cardiopharyngeal cell division patterns (Figure S3). While these effects did not account for the observed changes in gene expression, future studies will unravel FGF-

bioRxiv preprint doi: https://doi.org/10.1101/138701; this version posted January 12, 2018. The copyright holder for this preprint (which was not certified by peer review) is the author/funder. All rights reserved. No reuse allowed without permission.

MAPK-dependent and cardiopharyngeal-specific mechanisms governing the orientation and asymmetry of progenitor cell division (Kaplan et al., in preparation).

Transcriptional consequences of differential FGF-MAPK signaling.

Differential FGF-MAPK signaling rapidly impacts cell-specific gene expression, we thus surmise that transcriptional effectors are dynamically regulated. Even though we have not formally identified the downstream DNA-binding transcription factor (see discussion below), it is conceivable that the phosphorylated forms of either transcriptional effector could persist through cell division upon maintenance of FGF-MAPK activity. However, we have shown that continuous MAPK activity is needed following each division. Therefore, we must invoke elusive phosphatase activities, such as dual-specificity phosphatases (DUSPs; (Patterson et al., 2009), which would reset transcriptional effectors to a dephosphorylated state, thus rendering steady-state FGF-Ras-MAPK inputs necessary.

Systematic dephosphorylation of FGF-MAPK transcriptional effectors is particularly important for heart fate specification. As shown in our companion paper (Wang et al., 2017), whole genome analyses indicate that heart-specific *de novo* gene expression requires MAPK inhibition (Wang et al., 2017). The molecular mechanisms remain elusive, but one simple possibility is that, lest fate-restricted heart precursors inhibit MAPK activity, they will activate *Tbx1/10* and *Ebf*, which will block the cardiac program (Razy-Krajka et al., 2014; Stolfi et al., 2010; Wang et al., 2013).

Finally, we previously proposed that repressor inputs from Nk4/Nkx2-5 are needed in the second heart precursors to avoid ectopic activation of *Ebf* (Wang et al., 2013). The observation that *Nk4* transcripts are detected in all cardiopharyngeal cells opened the question as to how *Ebf* would escape repression by Nk4 in the ASMFs. Differential MAPK activity offers an intriguing possibility: for instance, Nk4/Nkx2.5-mediated

bioRxiv preprint doi: https://doi.org/10.1101/138701; this version posted January 12, 2018. The copyright holder for this preprint (which was not certified by peer review) is the author/funder. All rights reserved. No reuse allowed without permission.

566 repression in other species involves the co-repressor Groucho/TLE (Choi et al., 1999),
567 which is strongly expressed in the cardiopharyngeal mesoderm (Razy-Krajka et al.,
568 2014); and, in flies, MAPK-mediated phosphorylation of Groucho inhibits its repressor
569 function (Cinnamon et al., 2008; Cinnamon and Paroush, 2008; Hasson et al., 2005).
570 Therefore, it is possible that persistent MAPK signaling dampens Groucho/TLE-
571 mediated repressive inputs on cell-specific regulatory genes like *Ebf*. Future studies will
572 determine whether such mechanisms provide bistable switches underlying MAPK-
573 dependent fate choices in the cardiopharyngeal mesoderm.
574
575 **Temporal deployment of the pharyngeal muscle network**
576 The localized and successive activation of *Tbx1/10* and *Ebf* in STVCs, and ASMFs,
577 respectively, are important features of the cardiopharyngeal network that permit the
578 emergence of diverse cell fates: first and second heart precursors, and atrial siphon
579 muscle precursors. Experimental misexpression of Ebf throughout the
580 cardiopharyngeal mesoderm suffice to inhibit heart development (Razy-Krajka et al.,
581 2014; Stolfi et al., 2010), illustrating the importance of *Ebf* restriction to the ASMF for
582 the emergence of first and second heart precursors.
583 Our analyses indicate that the sequential activations of *Hand-r*, *Tbx1/10* and *Ebf* is
584 encoded in the feed-forward structure of this sub-circuit, whereas the continuous
585 requirement for MAPK inputs and their progressive exclusion from heart progenitors
586 restrict the competence to activate *Tbx1/10* and *Ebf* to the most lateral cells, after each
587 division. Our model implies that each gene may directly respond to transcriptional
588 inputs from MAPK signaling. We have not formally identified the transcription
589 factors(s) that mediate the transcriptional response to FGF-MAPK signaling. However,
590 multipotent cardiopharyngeal progenitors express *Ets1/2* and *Elk*, two common
591 transcriptional effectors of FGF/MAPK signaling in *Ciona* (Bertrand et al., 2003;

bioRxiv preprint doi: https://doi.org/10.1101/138701; this version posted January 12, 2018. The copyright holder for this preprint (which was not certified by peer review) is the author/funder. All rights reserved. No reuse allowed without permission.

592 Christiaen et al., 2008; Davidson et al., 2006; Gainous et al., 2015), and Ets1/2 has been
593 implicated in the initial FGF-MAPK-dependent induction of multipotent TVCs
594 (Christiaen et al., 2008; Davidson et al., 2006), and its expression is also progressively
595 restricted to the lateral-most progenitors following each division (Razy-Krajka et al.,
596 2014). Taken together, Ets1/2 and, to some extend, Elk are intriguing candidate
597 transcriptional effectors of FGF/MAPK signaling in cardiopharyngeal development.
598 The binding preferences of Ets-family factors have been extensively studied in
599 *Ciona*, and they do not depart markedly from conserved Ets-family binding sites with a
600 GGAW core (Bertrand et al., 2003; Farley et al., 2015; Farley et al., 2016; Gueroult-
601 Bellone et al., 2017; Khoueiry et al., 2010). Putative Ets-family binding sites in the TVC-
602 specific *Hand-r* enhancer are conserved between *Ciona intestinalis* and its sibling
603 species *C. robusta* and *C. savignyi*, and necessary for its activity in reporter assays
604 (Woznica et al., 2012). Similarly, minimal STVC and ASM enhancers for *Tbx1/10* and
605 *Ebf*, respectively, contain conserved putative Ets-family binding sites, which contribute
606 to proper reporter gene expression in transfection assays (Figure S5; (Razy-Krajka et al.,
607 2014; Wang et al., 2013) and data not shown). Taken together, these observations
608 suggest that the proposed feed-forward sub-circuit involves direct transcriptional inputs
609 from FGF-MAPK-regulated Ets-family factors on the cardiopharyngeal enhancers of
610 *Hand-r*, *Tbx1/10* and *Ebf*.
611
612 Whereas the regulatory architecture of the MAPK; Hand-r; Tbx1/10; Ebf sub-circuit
613 explains the sequence of activation events, it is also crucial for its correct deployment,
614 and the generation of diverse cell identities, that genes are not fully activated before
615 successive cell divisions. While divisions are not absolutely required for *Ebf* to
616 eventually turn on, cell cycle progression appears to entrain the deployment of this
617 network, especially for *Tbx1/10* and *Ebf* activation in STVCs and ASMFs, respectively.

bioRxiv preprint doi: https://doi.org/10.1101/138701; this version posted January 12, 2018. The copyright holder for this preprint (which was not certified by peer review) is the author/funder. All rights reserved. No reuse allowed without permission.

These observations imply that the intrinsic dynamic of the network is slower than observed. This allows first and second heart precursors to be born prior to the onset of *Tbx1/10* and *Ebf*, respectively. The latter sequence is essentially for the heart progenitors to escape the anti-cardiogenic effects of Tbx1/10 (Wang et al., 2013), and Ebf (Razy-Krajka et al., 2014).

Initial *Ebf* expression in early ASMFs is also labile and MAPK-dependent for approximately one hour. This continued requirement for MAPK inputs ensures that, in the rare instances when *Ebf* expression starts in the multipotent STVC progenitors and/or expands to the nascent SHPs, inhibition of MAPK shuts off *Ebf* expression before it reaches the levels needed for commitment to an ASM fate. Indeed, our results indicate that, once *Ebf* mRNAs have accumulated to high levels, its expression becomes auto-regulative and MAPK-independent. We surmise that this transition coincides with a fundamental switch from a multipotent cardiopharyngeal state to a committed pharyngeal muscle identity.

From this standpoint, the observed entrainment of *Ebf* expression by the cell cycle can be seen as acceleration of the transition to commitment following asymmetric division of multipotent progenitors. Although the mechanisms remain elusive, it is likely that this requires the M/G1 transition, as the G1 phase has been shown to be particularly conducive to the expression of fate-specific regulators in mammalian pluripotent stem cells (Dalton, 2015; Pauklin et al., 2016; Pauklin and Vallier, 2013; Soufi and Dalton, 2016).

Conserved dual effects of FGF-MAPK signaling on heart development in chordates

Previous studies highlighted how FGF-MAPK signaling is necessary along side Mesp during early cardiac development in *Ciona* (Christiaen et al., 2008; Davidson, 2007;

bioRxiv preprint doi: https://doi.org/10.1101/138701; this version posted January 12, 2018. The copyright holder for this preprint (which was not certified by peer review) is the author/funder. All rights reserved. No reuse allowed without permission.

644 Davidson et al., 2006), and how this early requirement also exists in vertebrates (Abu-
645 Issa et al., 2002; Alsan and Schultheiss, 2002; Barron et al., 2000; Brand, 2003; Reifers
646 et al., 2000; Zaffran and Frasch, 2002). We now know that these early FGF-MAPK
647 inputs induce and maintain multipotent cardiopharyngeal states in *Ciona*, including the
648 *Tbx1/10*+ multipotent progenitors that eventually produce the second heart lineage
649 ((Razy-Krajka et al., 2014; Stolfi et al., 2010; Wang et al., 2013), (Wang et al., 2017) and
650 this study). Similarly, in vertebrates, regulatory interplay between Fgf8 and Fgf10
651 signaling and Tbx1 is required for development of both pharyngeal arch and second
652 heart field derivatives, presumably in part by maintaining an undifferentiated and
653 proliferative state (Abu-Issa et al., 2002; Aggarwal et al., 2006; Brown et al., 2004;
654 Chen et al., 2009; Hu et al., 2004; Ilagan et al., 2006; Kelly and Papaioannou, 2007;
655 Park et al., 2006; Park et al., 2008; Vitelli et al., 2002b; Watanabe et al., 2010;
656 Watanabe et al., 2012). In fish, FGF signaling is necessary for cardiomyocyte addition at
657 the arterial pole, in a manner reminiscent of its role in second heart field development
658 (de Pater et al., 2009; Lazic and Scott, 2011). Notably, FGF signaling acts in successive
659 phases, and its inhibition is necessary for final myocardial specification and
660 differentiation (Hutson et al., 2010; Marques et al., 2008; Tirosh-Finkel et al., 2010;
661 van Wijk et al., 2009). Conversely, continued FGF signaling beyond the multipotent
662 mesodermal progenitor stages was shown to promote smooth muscle and epicardial
663 differential in the heart (Hutson et al., 2010; van Wijk et al., 2009), and also myoblast
664 specification and/or skeletal muscle differentiation in the head, with the expression of
665 FGF ligands being maintained in the pharyngeal arches (Bothe et al., 2011; Buckingham
666 and Vincent, 2009; Michailovici et al., 2015; Michailovici et al., 2014; von Scheven et
667 al., 2006). Taken together, these and our data suggest that FGF-MAPK signaling plays
668 evolutionary conserved roles during chordate cardiopharyngeal development, by
669 promoting the specification of successive mesodermal and *Tbx1*+ multipotent states,

bioRxiv preprint doi: https://doi.org/10.1101/138701; this version posted January 12, 2018. The copyright holder for this preprint (which was not certified by peer review) is the author/funder. All rights reserved. No reuse allowed without permission.

and a fate-restricted non-cardiac muscle identity, while MAPK inhibition is required for myocardial specification and differentiation in the first and second heart field, successively.

bioRxiv preprint doi: https://doi.org/10.1101/138701; this version posted January 12, 2018. The copyright holder for this preprint (which was not certified by peer review) is the author/funder. All rights reserved. No reuse allowed without permission.

673 **Material and methods**

674 **Animals, electroporations, and chemical treatments**

675 Gravid wild *Ciona intestinalis* type A, now called *Ciona robusta* (Pennati et al., 2015),
676 were obtained M-REP (Carlsbad, CA, USA), and kept under constant light to avoid
677 spawning. Gametes from several animals were collected separately for *in vitro* cross-
678 fertilization followed by dechorionation and electroporation as previously described
679 (Christiaen et al., 2009a, b). Different quantities of plasmids were electroporated
680 depending on the constructs. Typically, 50 µg of DNA was electroporated for NLS::lacZ
681 or plain mCherry driving constructs but only 15 µg for *Mesp-1>H2B::mCherry*. For
682 perturbation constructs, 70 µg were usually electroporated, except for
683 *Mesp>NLS::Cas9::NLS* (30 µg) and pairs of U6>sgRNA plasmids (25 µg each). U0126
684 (Cell Signaling Technology, Danvers, MA) was used at 5µM in artificial seawater from a
685 stock solution of 20mM in DMSO. Cytochalasin B (Sigma, Saint Louis, MO) was used at
686 ~3 µg/mL from a 10 mg/mL stock solution in DMSO as previously performed (Jeffery et
687 al., 2008). Control embryos were incubated in parallel with corresponding
688 concentrations of DMSO alone.

689

690 ***In situ* hybridization**

691 *In situ* hybridizations were carried out essentially as described previously (Christiaen et
692 al., 2009c; Razy-Krajka et al., 2014), using DIG labeled riboprobes, anti-DIG-POD Fab
693 fragments (Roche, Indianapolis, IN), and Tyramide Amplification Signal coupled to
694 Fluorescein (Perkin Elmer, MA). Reporters expressed in the lineage of interest were
695 marked using anti-ß-galactosidase monoclonal mouse antibody (1:1000; Promega,
696 Fitchburg, WI) or anti-mCherry rabbit polyclonal antibody (1:500; BioVision 5993-
697 100), respectively targeted with anti-mouse or anti-rabbit secondary antibody coupled
698 with Alexa 648 (1:500; Invitrogen, Carlsbad, CA). The different probes used in this

bioRxiv preprint doi: https://doi.org/10.1101/138701; this version posted January 12, 2018. The copyright holder for this preprint (which was not certified by peer review) is the author/funder. All rights reserved. No reuse allowed without permission.

699 study were described previously (Razy-Krajka et al., 2014; Stolfi et al., 2010; Wang et
700 al., 2013).
701
702 **dpERK/mcherry double fluorescent immunostaining**
703 Samples were fixed, as for *in situ* hybridizations, in MEM-PFA with Tween 20 (0.05%)
704 but only for 30 minutes at room temperature, washed three times in PBSt (Tween 20
705 0.01%) for 10 minutes, gradually dehydrated every 10 minutes in Ethanol/PBS series
706 (33%, 50%, 80%) and Methanol 100%. Samples were then gradually rehydrated every
707 10 minutes in Methanol/PBSt series, rinsed three times in PBSt, permeabilized with
708 PBS Triton-100 (0.2%) for 30 minutes and incubated for 2 hours at room temperature
709 with anti-dpERK mouse monoclonal antibody (1:200; Sigma, Saint Louis, MO) and
710 anti-mCherry polyclonal antibody from rabbit (1:500; Biovision, Milpitas, CA) in PBS
711 0.01% Triton-100 (T-Pbs) supplemented with 2% normal goat serum. Samples were
712 then washed three times in T-PBS and incubated in anti-mouse and anti-rabbit
713 antibodies (1 :500 each), respectively coupled with Alexa 488 and Alexa 568
714 (Invitrogen, Carlsbad, CA), overnight at 4°C or for 2 hours at room temperature.
715 Finally, samples were rinsed three times in T-PBS for 15 minutes and mounted in
716 Prolong Gold (Molecular Probes, Eugene, OR).
717
718 **Molecular cloning**
719
720 Coding sequences for wild-type M-Ras (KH.L172.2), Mek1/2 (KH.L147.22), Cdkn1b.a
721 (Cdkn1b, KH.C14.564), and Cdkn1b.b (Noto16, KH.S643.6) were PCR-amplified from
722 cDNA libraries prepared by reverse transcription of total RNA from mixed
723 developmental stages. Insertion of the products into expressing vectors was performed
724 using regular restriction/ligation or In-fusion (Clontech, Mountain View, CA)
725 procedure. Oligonucleotide directed mutagenesis or two-step overlap PCRs were used to

bioRxiv preprint doi: https://doi.org/10.1101/138701; this version posted January 12, 2018. The copyright holder for this preprint (which was not certified by peer review) is the author/funder. All rights reserved. No reuse allowed without permission.

generate the point mutated forms M-Ras^{G22V} and Mek^{S220E,S216D} from the corresponding wild-type sequences. We also used oligonucleotide directed mutagenesis to generate mismatches in the PAM sequences adjacent to the sgRNA targets for Hand-r (153C>T 574C>T for Hand-r^{PAMmis}) and Tbx1/10 (325G>A and 579G>A for Tbx1/10^{PAMmis}). Due to the absence of a correct PAM sequence (NGG, (reverse complement CCN)), overexpressed Hand-r^{PAMmis} and Tbx1/10^{PAMmis} are resistant to the Cas9 nuclease activity. We also used oligonucleotide directed mutagenesis to generate the mutations in two putative Ets binding sites from the corresponding wild-type sequence of the *Tbx1/10* enhancer element: -3646TC>CT -3638GA>AG upstream from the initiation codon (E1 and E2 in Figure S5 C, respectively). Primer sequences are listed in Supplementary Table 1.

CRISPR/Cas9-mediated loss of Hand-r function

The pair of single guide RNA (sgRNA) targeting Tbx1/10 (sgTbx1/10) has been validated previously (Tolkin and Christiaen, 2016). Rescue of the Tbx1/10 loss-of-function was achieved by TVC-specific overexpression of Tbx1/10^{PAMmis} driven by a *Foxf* enhancer (Foxf-1>Tbx1/10^{PAMmis}). For Hand-r loss of function, sgRNAs were first designed to avoid genomic off-targets and tested as described (Gandhi et al., 2017b). In short, sgRNA expressing cassettes (U6>sgRNA) were assembled by single step overlap PCR. Individual PCR products (~25 µg) were electroporated with EF1a>NLS::Cas9::NLS (30µg) , Myod905>Venus (50 µg), driving ubiquitous expression of Cas9 and a widely expressed fluorescent reporter construct, respectively. Efficient electroporation was confirmed by observation of fluorescence before genomic DNA extraction around 16 hpf (18°C) using QIAamp DNA Micro kit (Qiagen, German Town, MD). Mutagenesis efficacy of individual sgRNAs, as a linear function of Cas9-induced indel frequency, was

bioRxiv preprint doi: https://doi.org/10.1101/138701; this version posted January 12, 2018. The copyright holder for this preprint (which was not certified by peer review) is the author/funder. All rights reserved. No reuse allowed without permission.

752 estimated from electrophoregrams following Singer sequencing of the targeted regions
753 amplified from extracted genomic DNA by PCR. Result of the relative quantification of
754 the indel frequency ("corrected peakshift" of 22% and 24%) was considered high enough
755 for both sgRNAs targeting Hand-r, which were finally selected. The corresponding
756 cassettes were cloned into plasmid for repeated electroporations to study the loss of
757 function of Hand-r. Rescue of Hand-r loss-of-function was achieved by overexpression
758 of Hand-r^{PAMmis} driven by a Foxf TVC specific enhancer (Foxf-1>Hand-r^{PAMmis}). In order
759 to control the specificity of the CRISPR/Cas9 system, sgRNAs targeting *Neurogenin*, a
760 gene not expressed in the TVC and their progeny, was electroporated in parallel.
761 Sequences of the DNA targets and oligonucleotides used for the sgRNAs are listed in
762 Supplementary Table 1.
763
764 **_Tbx1/10_ enhancer and _cis_-regulatory analysis**
765 To isolate the minimal STVC-specific element of *Tbx1/10*, we used conserved non
766 coding sequences between *Ciona robusta* and *Ciona savignyi* as a guide for molecular
767 dissection (Figure S5 A, http://genome.lbl.gov/vista/index.shtml; (Frazer et al., 2004)).
768 We cloned a full-length *cis*-regulatory DNA construct (~7kbp) that was analyzed by
769 introducing large deletions to map the functional elements. We found a fragment of
770 1264 bp, that we called T6, located at -4682 bp upstream from the initiation codon that
771 was sufficient for STVC expression as well as in the mesenchyme and endoderm of the
772 reporter gene (Figure S5 A, B). 5' deletions of the T6 element show that the main *cis*-
773 regulatory elements required exclusively for STVC expression map in a 575 bp element,
774 which we called T12, at -4116 bp upstream from the initiation codon sufficient (Figure
775 S5A). The sequence of this element, which we called *T12*, reveals the presence of
776 putative Ets1/2 binding sites (Figure S5C) that were predicted using JASPAR (Khan et
777 al., 2017) and CisBP (Weirauch et al., 2014) databases. The minimal *Tbx1/10* STVC-

bioRxiv preprint doi: https://doi.org/10.1101/138701; this version posted January 12, 2018. The copyright holder for this preprint (which was not certified by peer review) is the author/funder. All rights reserved. No reuse allowed without permission.

778 specific enhancer was further analyzed using point mutations of the candidate Ets1/2
779 sites with higher predicted scores (Figure S5D).
780
781 **Observation and imaging**
782 Samples were usually scored under a DM2500 epifluorescent microscope (Leica
783 Microsystems, Wetzlar, Germany). Imaging was performed using a TCS SP8 X inverted
784 confocal microscope equipped with a white light laser, AOBS and HyD detectors (Leica
785 Microsystems).
786
787 **Acknowledgement**
788 We thank Robert Kelly (Université Aix-Marseille, CNRS, France) for feedbacks on the
789 manuscript. We are grateful to Alberto Stolfi for collaborative inputs throughout the
790 project. We thank Farhana Salek and Kristyn Millan for technical support. This project
791 was funded by NIH/NHLBI R01 award HL108643, and trans-Atlantic network of
792 excellence award 15CVD01 from the Leducq Foundation to L.C.
793

bioRxiv preprint doi: https://doi.org/10.1101/138701; this version posted January 12, 2018. The copyright holder for this preprint (which was not certified by peer review) is the author/funder. All rights reserved. No reuse allowed without permission.

Figures

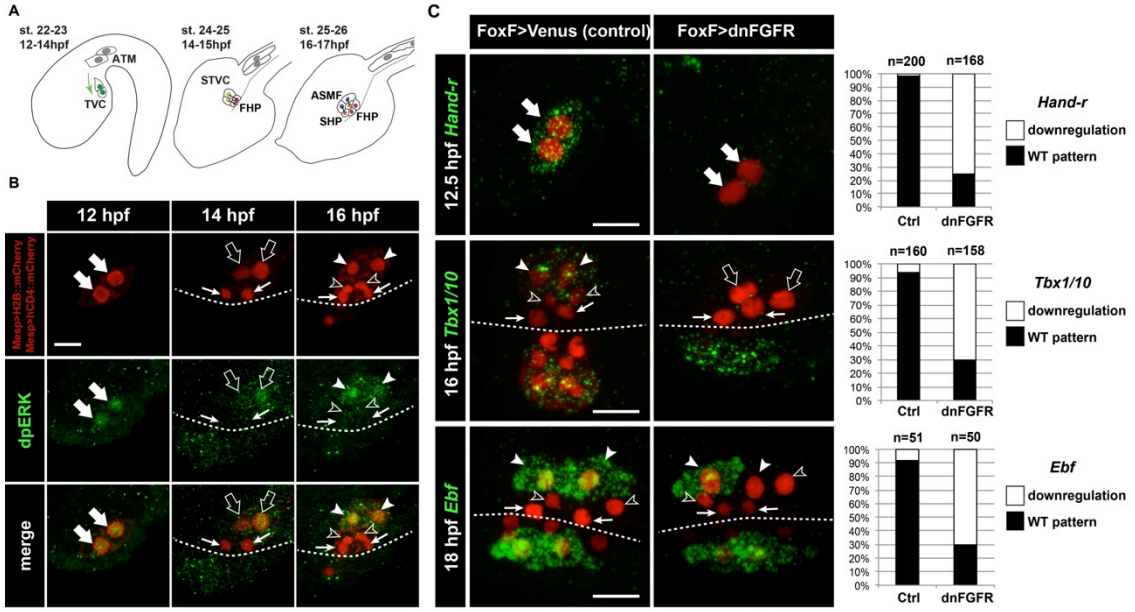

Figure 1. Spatio-temporal restriction of ERK activity reflects FGF requirement for the specification of cardiopharyngeal progenitors. (**A**) Schematic of *Ciona* development showing asymmetric cell divisions and resulting cell fates of the cardiopharyngeal mesoderm (CPM). Embryonic and larval stages (St) according to (Hotta et al., 2007) with hours post fertilization (hpf) at 18°C. Anterior tail muscle (ATM, gray), trunk ventral cell (TVC, green), secondary TVC (STVC, green), first heart precursor (FHP, red), second heart precursor (SHP, orange), atrial siphon founder cell (ASMF, blue). Black bars link sister cells. Dashed lines: ventral midline. The first stage presents a quasi-lateral view while the second and third stages present quasi-ventral views. Anterior is to the left. Scale bar, 50 µm. (**B**) ERK activity visualized by anti-dpERK antibody (green). TVCs and their progeny are marked by mCherry driven by *Mesp* and revealed by anti-mCherry antibody (red). H_2B::mCherry and hCD4::mCherry accumulate in the nuclei and at the cell membrane, respectively. Arrowheads indicate STVCs and ASMFs at 14 and 16 hpf, respectively. Arrows indicate FHPs and open arrowheads mark SHPs. Anterior to the left. Scale bar, 10 µm. See also Figure S1 for broader time series of dpERK immunostaining in the B7.5 lineage. (**C, D**) TVC-specific overexpression of dnFGFR induces loss of expression of key lateral CPM markers visualized by *in situ* hybridization. (**C**) Representative expression patterns of key CPM genes (*Hand-related*, *Tbx1/10*, *Ebf*) in control embryos (Ctrl, electroporated with Foxf(TVC):bpFOG-1>Venus) and TVC-specific dnFGFR expression (electroporated with *Foxf(TVC):bpFOG-1>dnFGFR::mCherry*) individuals. TVCs and progeny are marked with *Mesp>NLS::lacZ* (red). Loss of expression in half of the TVC progeny, as presented for *Ebf*, is assumed to be due to left-right mosaicism. Arrowheads mark the ASMFs. Anterior is to the left. Scale bar, 10 µm. (**D**) Corresponding histograms with the phenotype proportions. For simplicity, loss of gene expression in half or all of the TVCs and their progeny were combined in the same category. "n" corresponds to the number of individual halves documented per condition.

bioRxiv preprint doi: https://doi.org/10.1101/138701; this version posted January 12, 2018. The copyright holder for this preprint (which was not certified by peer review) is the author/funder. All rights reserved. No reuse allowed without permission.

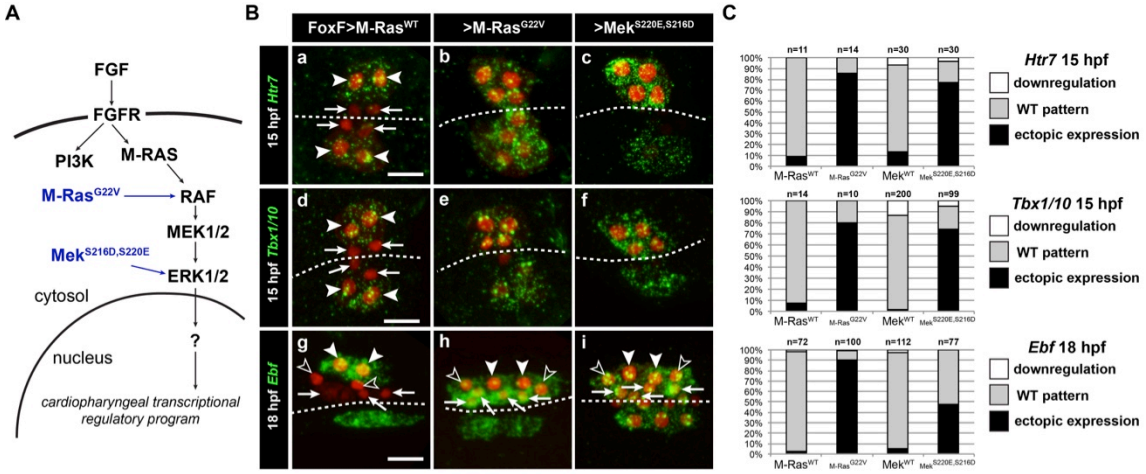

Figure 2. Constitutively active M-Ras and MEK are sufficient to impose a pharyngeal muscle fate in the cardiopharyngeal lineage. (**A**) Diagram of the FGF/MAPK transduction pathway with constitutive activation by M-Ras^{G22V} and MEK^{S216D,S220E} mutants. (**B**) Expression patterns of markers of the lateral TVC progeny, *Htr7* (a, b, c,), *Tbx1/10* (d, e, f) and *Ebf* (g, h, i), visualized by *in situ* hybridization following TVC-specific over-expression of M-Ras^{WT} (as control), M-Ras^{G22V} and MEK^{S216D,S220E}. M-Ras^{WT} overexpression (a, d, g) does not alter the wild-type spatial expression patterns of *Htr7*, *Tbx1/10* and *Ebf* in lateral TVC derivatives (STVC and ASMF) and excluded from the median heart precursors. TVC-specific over-expression of M-Ras^{G22V} (b, e, h) or MEK^{S216D,S220E} (c, f, i) induces ectopic expression of STVC and/or ASMF markers (*Htr7*, *Tbx1/10* and *Ebf*) in the more median cells, that normally form cardiac precursors. Arrowheads indicate STVCs and ASMFs at 15 and 18 hpf, respectively. Arrows indicate FHPs and open arrowheads mark SHPs. At 18 hpf, the FHPs start dividing or have divided into 4 cells. Anterior to the left. Scale bar, 10 μm. (**C**) Corresponding histograms: Larvae with TVC-specific over-expression of MEK^{WT} retain the wild-type expression patterns. For simplicity, ectopic expressions in half to all of the cardiac precursors were combined in the same phenotype category. "n" corresponds to the number of embryo halves documented per condition. See also Figure S2.

bioRxiv preprint doi: https://doi.org/10.1101/138701; this version posted January 12, 2018. The copyright holder for this preprint (which was not certified by peer review) is the author/funder. All rights reserved. No reuse allowed without permission.

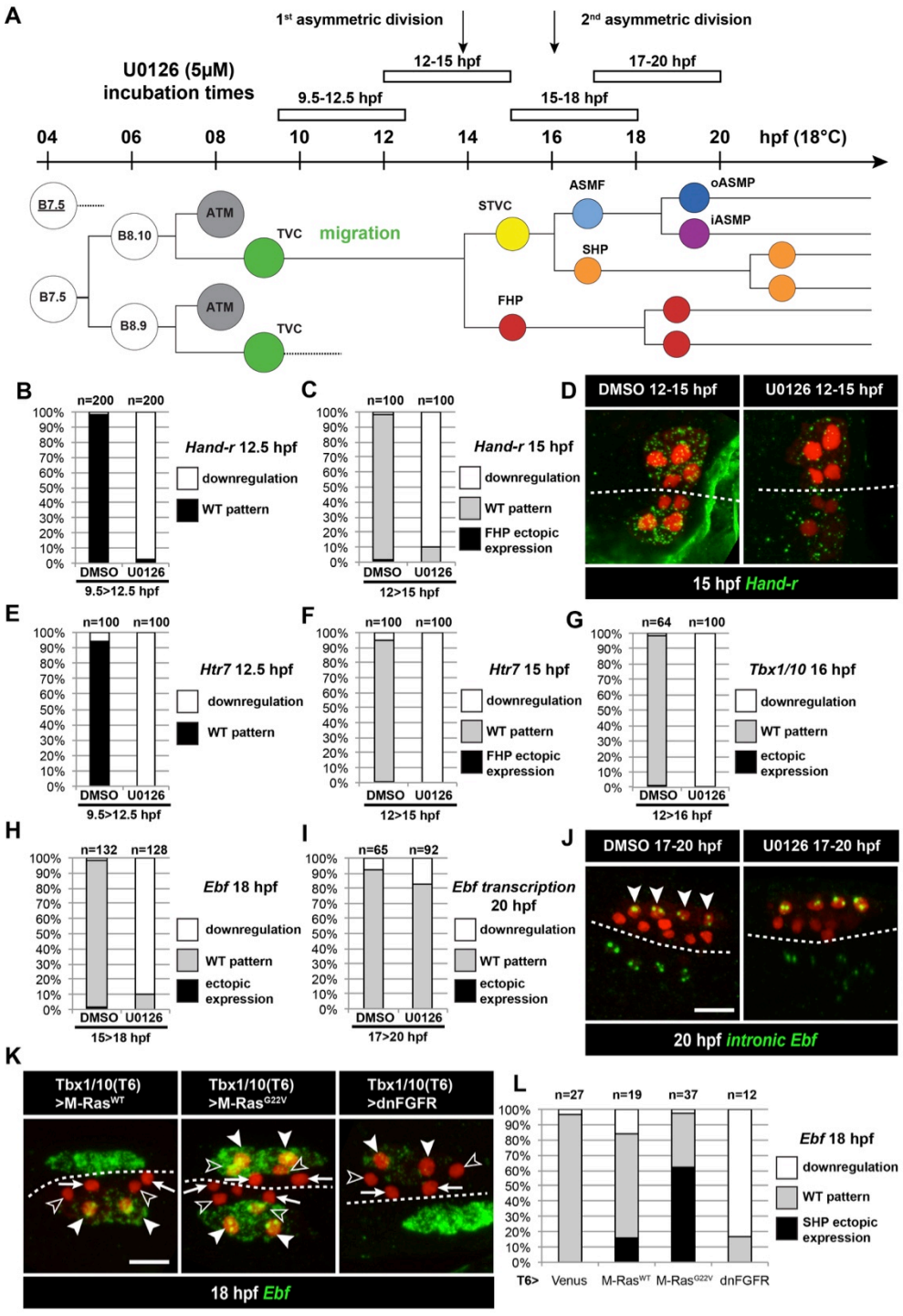

Figure 3. Temporal requirement for MAPK activity permits the progressive deployment of the cardiopharyngeal regulatory program. (**A**) Summary of the CPM cell lineage showing the different U0126 treatments with regard to the timing of the cell divisions. Abbreviations and color codes as in Figure 1. (**B, C**) Proportions of embryo halves with wild-type or downregulated expression of *Hand-r* at 12.5 hpf (B) and 15 hpf (C) following 3-hour incubations in U0126 (with DMSO as control treatment). (**D**) *Hand-r* expression visualized by *in situ* hybridization at 15 hpf in control (DMSO treated) and U0126 treated embryos. In control embryos, *Hand-r* remains expressed in the STVCs and downregulated in the FHPs. In U0126 (12-15 hpf) treated embryos, downregulation of *Hand-r* expression is observed throughout the TVC progeny (STVCs and FHPs), suggesting inhibition of transcription and inheritance of remnant

bioRxiv preprint doi: https://doi.org/10.1101/138701; this version posted January 12, 2018. The copyright holder for this preprint (which was not certified by peer review) is the author/funder. All rights reserved. No reuse allowed without permission.

transcripts following TVC divisions. (**E, F**) Proportions of embryo halves with wild-type or downregulated expression of *Htr7* at 12.5 hpf (E) and 15 hpf (F) following 3-hour incubations in U0126 (with DMSO as control treatment). (**G**) Proportions of larvae with wild-type expression or downregulated expression of *Tbx1/10* at 16 hpf following 4-hour incubation in U0126 (with DMSO as control). (**H**) Proportions of larvae with wild-type or downregulated expression of *Ebf* at 18 hpf following a three hour incubation in U0126 (with DMSO as control). (**I**) Proportions of larvae with wild-type or downregulated transcription of *Ebf* at 18 hpf following a three hour incubation in U0126 (DMSO as vehicle control). (**J**) Pattern of nascent *Ebf* transcripts visualized by *in situ* hybridization with intronic probes (green) at 20 hpf. The nuclear dots reveal the active transcription sites in the four ASMPs per side in larvae, both control/DMSO- and U0126-treated from 17 to 20 hpf. (**K**) *Ebf* expression (green) in 18hpf larvae expressing control M-Ras^{WT}, constitutively active M-Ras^{G22V} or dominant negative dnFGFR under the control of the T12 element, an STVC-specific *Tbx1/10* enhancer. Arrows: first heart precursors (FHP); open arrowhead: second heart precursors (SHPs); closed arrowheads: ASM founder cells (ASMFs); dotted line: midline. (**L**) Proportions of larvae with wild-type or downregulated expression of *Ebf* at 18 hpf in larvae with Venus (control), M-Ras^{WT}, M-Ras^{G22}, or dnFGFR driven by *Tbx1/10 cis*-regulatory sequence and overexpressed in the STVCs. "n" : number of individual halves documented per condition.

bioRxiv preprint doi: https://doi.org/10.1101/138701; this version posted January 12, 2018. The copyright holder for this preprint (which was not certified by peer review) is the author/funder. All rights reserved. No reuse allowed without permission.

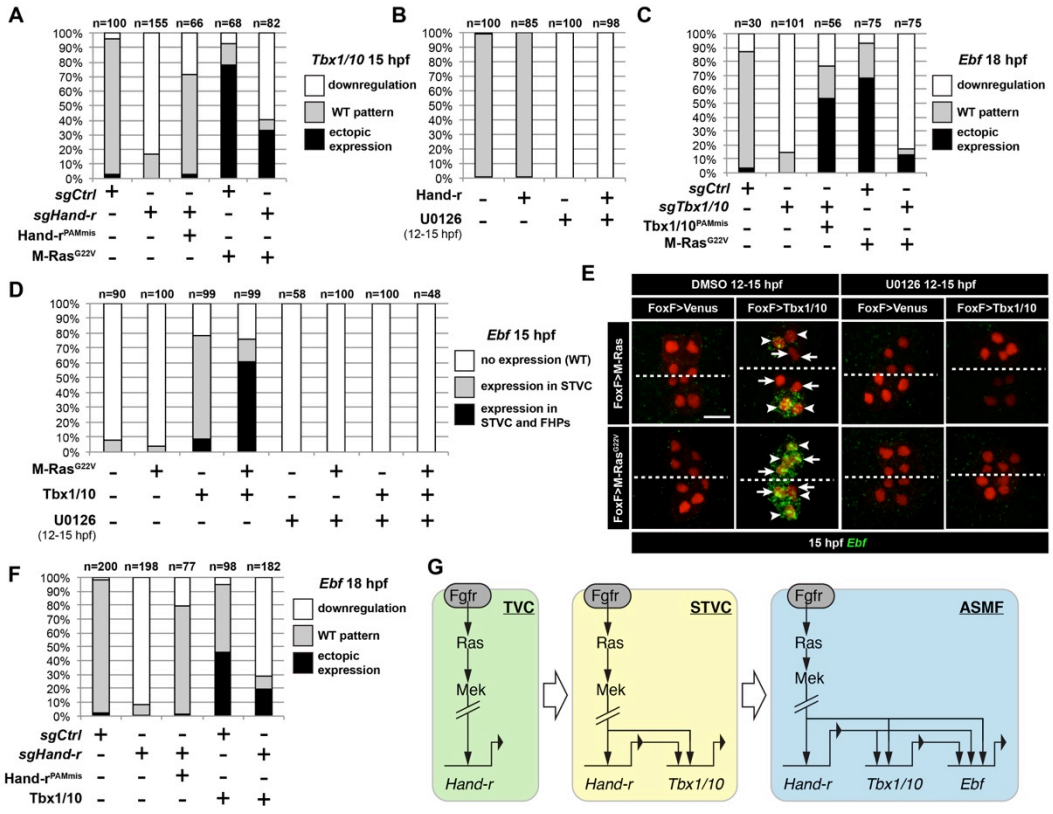

Figure 4. M-Ras/MAPK-driven feed-forward subcircuits control the successive activations of *Hand-r*, *Tbx1/10* and *Ebf*. (**A**) Proportions of embryo halves with indicated *Tbx1/10* expression patterns following TVC-specific CRISPR/Cas9-mediated mutagenesis of *Neurogenin/Neurog* as a control (*sgCtrl*), and Hand-r (*sgHand-r*). TVC-specific overexpression of a CRISPR/Cas9-resistant form of Hand-r with mutation in the PAM sequence (*Hand-r*^{PAMmis}) rescued *Tbx1/10* expression in the *sgHand-r* "background". TVC-specific overexpression of a constitutively active M-Ras mutant (M-Ras^{G22}) (control: M-Ras^{WT}) was sufficient to induce ectopic expression of *Tbx1/10* in the FHPs in *sgCtrl* embryos but not in *sgHand-r* embryos indicating that Hand-r is necessary for M-Ras-dependent activation of *Tbx1/10* transcription. (**B**) Proportions of embryo halves with indicated *Tbx1/10* expression patterns following TVC-specific overexpression of Hand-r or a neutral reporter (Venus) and treated from 12 to 15hpf with the MEK inhibitor U0126 (+) or with DMSO (-) as control. Hand-r overexpression is not sufficient to rescue loss of *Tbx1/10* expression due to MAPK inhibition indicating that M-Ras/MAPK activity is required in parallel of Hand-r expression to activate Tbx1/10 transcription in the TVC progeny. (**C**) Tbx1/10 is necessary downstream of M-Ras/MAPK activity to activate *Ebf* transcription in the TVC progeny. Shown are proportions of *Ebf* expression phenotypes following TVC-specific CRISPR/Cas9-mediated loss of *Tbx1/10* function (*sgTbx1/10*), with *Neurog*-targeting sgRNA as control (*sgCtrl*). Specificity of Tbx1/10 loss of function was validated through rescue of *Ebf* expression with TVC-specific overexpression of a CRISPR/Cas9 resistant form of *Tbx1/10* (Tbx1/10^{PAMmis}). Ectopic *Ebf* expression in SHPs in Tbx1/10^{PAMmis} larvae is explained by precocious misexpression of Tbx1/10 in the TVC as described in Wang et al, 2013. TVC-specific overexpression of M-Ras^{G22} (M-Ras^{G22}), with wild type M-Ras (M-Ras^{WT}) as control, was sufficient to induce ectopic expression of *Ebf* in the cardiac precursors in *sgCtrl* embryos but not in *sgTbx1/10* embryos indicating that Tbx1/10 is necessary for M-Ras-dependent activation of *Ebf* transcription. (**D, E**) Proportions (D) and examples (E) of 15hpf larvae halves showing indicated *Ebf* expression phenotypes in *sgCtrl* and *sgHand-r* CRISPR/Cas9 conditions combined with TVC-specific overexpression of a neutral reporter (Venus), Hand-r^{PAMmis}, or Tbx1/10, and with MEK inhibition by U0126 (+) or not (DMSO control (-)). Arrowhead: STVCs, Arrows: FHPs, dotted line: ventral midline (**F**) Loss of Hand-r function impaired the ability of Tbx1/10 to induce ectopic *Ebf* expression. For simplicity, ectopic expressions in half to all of the cardiac precursors were combined in the same phenotype category. "n=": number of individual halves documented per condition. (**G**) Summary model of the temporal deployment of FGF/MAPK-driven feed-forward sub-circuits leading to the sequential activations of *Tbx1/10* and *Ebf* in the STVCs and ASMFs, respectively.

bioRxiv preprint doi: https://doi.org/10.1101/138701; this version posted January 12, 2018. The copyright holder for this preprint (which was not certified by peer review) is the author/funder. All rights reserved. No reuse allowed without permission.

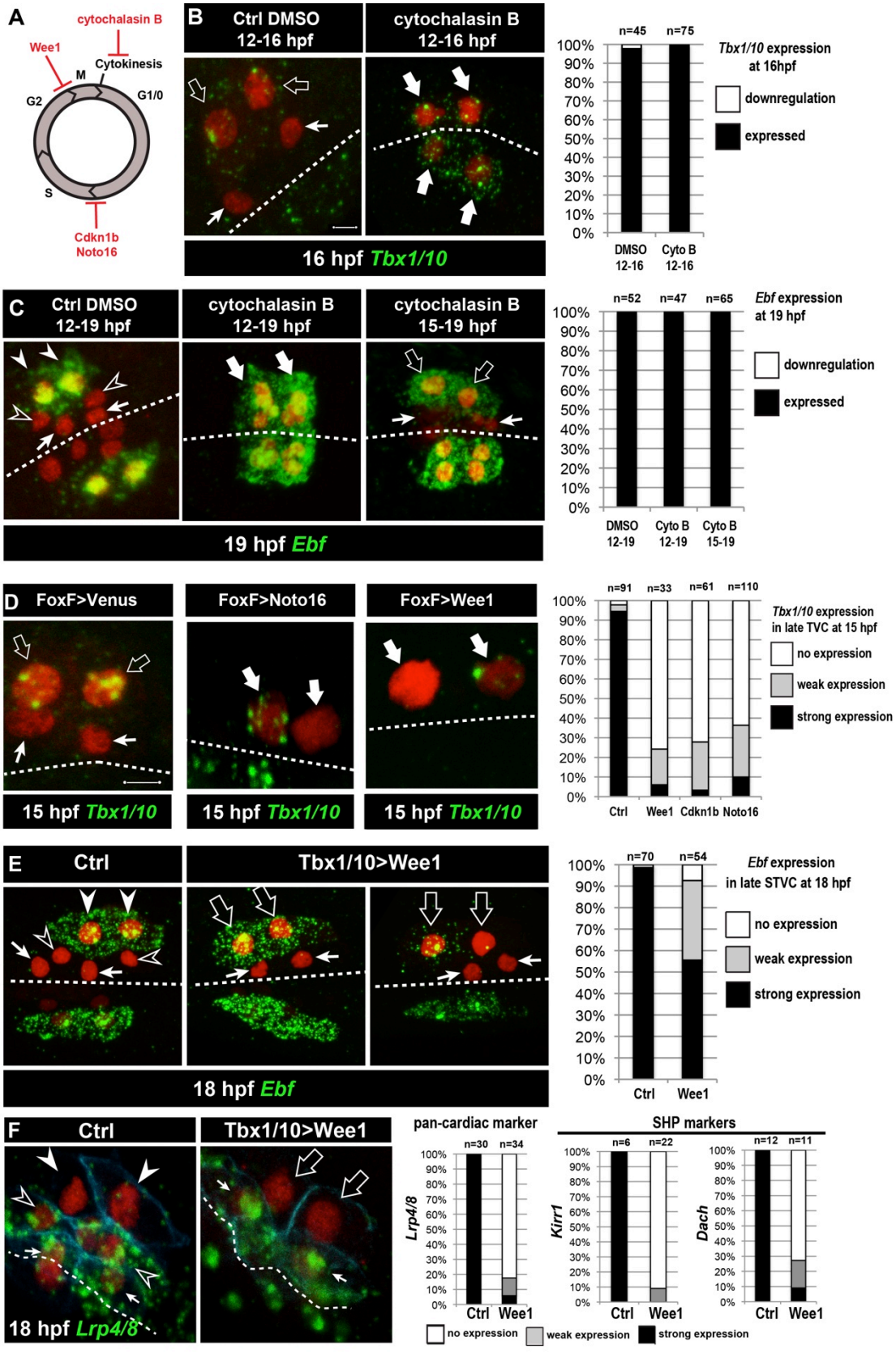

bioRxiv preprint doi: https://doi.org/10.1101/138701; this version posted January 12, 2018. The copyright holder for this preprint (which was not certified by peer review) is the author/funder. All rights reserved. No reuse allowed without permission.

Figure 5. Temporal deployment of the cardiopharyngeal network is partially coupled with cell cycle progression. (**A)** Schematic representation of the canonical eukaryotic cell cycle, and actions of the perturbations used in this study. (**B,C**) Tbx1/10 and Ebf expression at indicated time points, and following inhibition of cytokinesis by cytochalasin B treatment at indicated time points. Note that 15 to 19hpf treatment is applied AFTER the first division and birth the FHPs, which do not activate *Ebf* at 19hpf (right panel, arrows). (**D**) Inhibition of G1/S or G2/M blocks TVC division, and reduces *Tbx1/10* expression. Pictures shows TVCs that have divided in controls but not in experimental cells, with one cell occasionnally turning on *Tbx1/10*, but not the other. Left: the proportions of embryos showing strong *Tbx1/10* expression is substantially reduced compared to control embryos (e.g. Figure 1, and (Wang et al., 2013)). (**E**) Inhibition of G2/M in the STVCs by misexpression of Wee1 using the *Tbx1/10 T6* enhancer inhibits STVC division, and has a mild impact on *Ebf* expression at 18hpf. Open arrows indicate STVCs that have not divided, but express high (middle) or low (right) levels of *Ebf*. Left: control larva showing high *Ebf* expression in the ASMF (closed arrowheads), but neither in the SHPs (open arrowheads) nor in the FHPs (Arrows). (**F**) Misexpression of Wee1 using the *Tbx1/10 T6* enhancer (*Tbx1>Wee1*) inhibits STVC division. Right: the proportions of embryos showing strong *Lrp4/8, Kirr1* or *Dach* expression into late STVCs is reduced compared to SHPs in control embryos (T6>NLS::LacZ) at 18 hpf. Notably, the pan-cardiac marker *Lrp4/8* is still expressed in FHPs (arrows). Nuclei are marked in red with Mesp>NLS::lacZ, membranes in blue with Mesp>hCD4::mCherry, FHP labeled with arrows and SHP with arrowheads. 'n=', number of individual halves scored per condition. Scale bar, 5 µm. In all image panels, dotted line : ventral midline.

bioRxiv preprint doi: https://doi.org/10.1101/138701; this version posted January 12, 2018. The copyright holder for this preprint (which was not certified by peer review) is the author/funder. All rights reserved. No reuse allowed without permission.

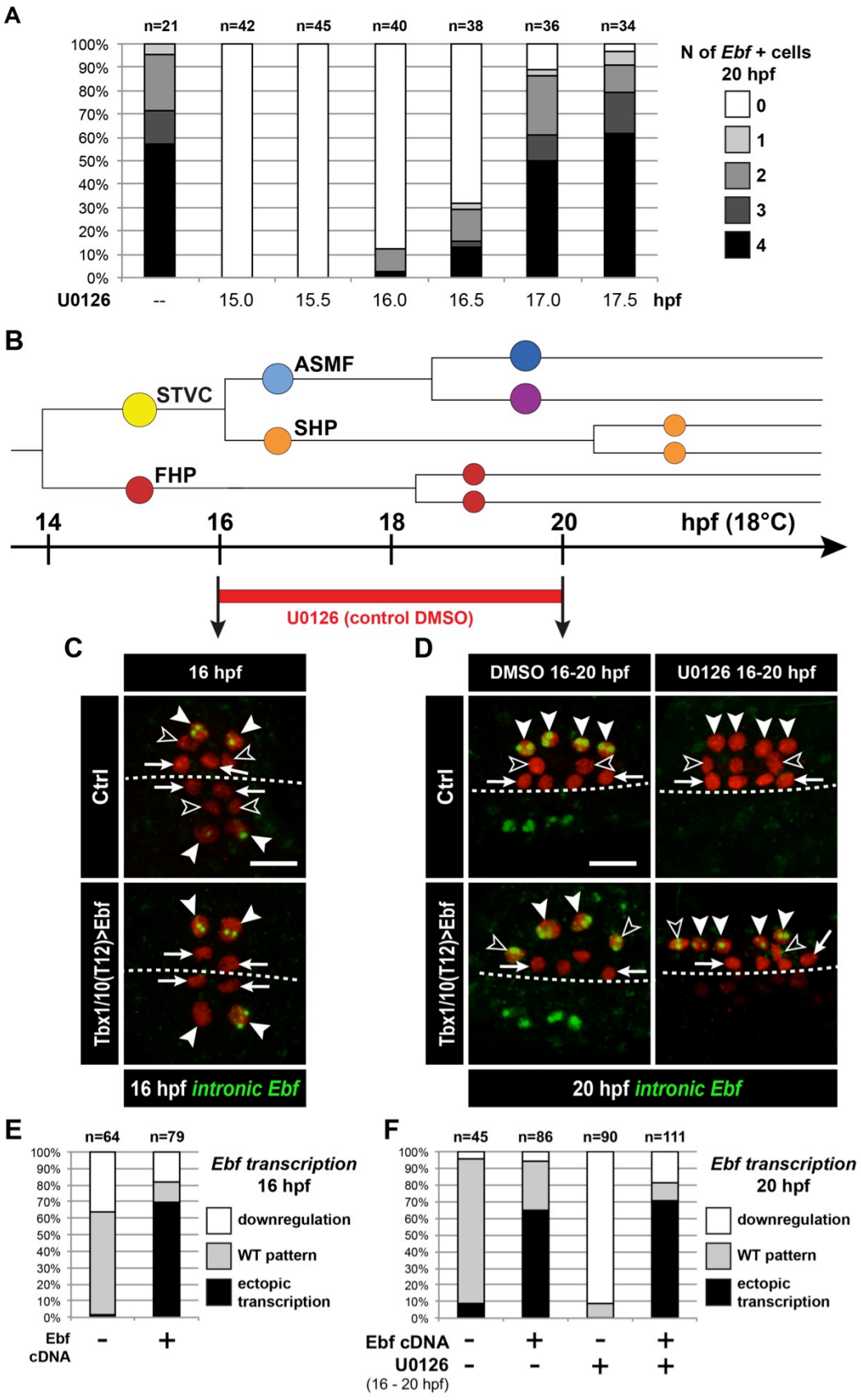

921

bioRxiv preprint doi: https://doi.org/10.1101/138701; this version posted January 12, 2018. The copyright holder for this preprint (which was not certified by peer review) is the author/funder. All rights reserved. No reuse allowed without permission.

Figure 6. *Ebf* regulation transitions from MAPK-dependent to autoregulative during the early phase of ASMF cycle. (**A**) Proportions of 20hpf larva halves showing the indicated number of Ebf-expressing cells following U0126 treatments started at the indicated time points. This indicates that, by 17hpf, Ebf expression, which started at ~16hpf, has become largely insensitive to loss of MAPK activity. (B) Summary lineage diagram and time scale indicating the approximate stages for U0126 and DMSO (control) treatments for the results shown in (C, D). (C) Control (Ctrl) and Ebf-misexpressing embryos fixed at 16hpf, prior to chemical treatments, and stained for nascent transcripts with an intronic *Ebf* probe. In controls, the ASMFs (solid arrowhead), but neither the SHPs (open arrowheads) nor the FHPs (arrows), actively transcribe *Ebf* (green nuclear dots). In Larvae misexpressing the Ebf cDNA under the control of the STVC-specific Tbx1/10 enhancer, divisions are delayed and STVCs (solid arrowheads) activated transcription of endogenous *Ebf* loci (green nuclear dots). (D) After 4 hours, U0126 treated ASMFs no longer transcribe Ebf (top right image, solid arrowheads), whereas control DMSO-treated ASMFs do (top left, green nuclear dots). Upon misexpression of the Ebf cDNA in the STVCs and derivatives, ongoing *Ebf* transcription is detected at 20hpf in both DMSO and U0126-treated cells, and it persists in both ASMFs (solid arrowheads), and SHPs (open arrowheads). (**E, F**) Proportions of larvae halves showing the indicated *Ebf* transcription patterns, in indicated experimental conditions, as illustrated in C and D, respectively.

bioRxiv preprint doi: https://doi.org/10.1101/138701; this version posted January 12, 2018. The copyright holder for this preprint (which was not certified by peer review) is the author/funder. All rights reserved. No reuse allowed without permission.

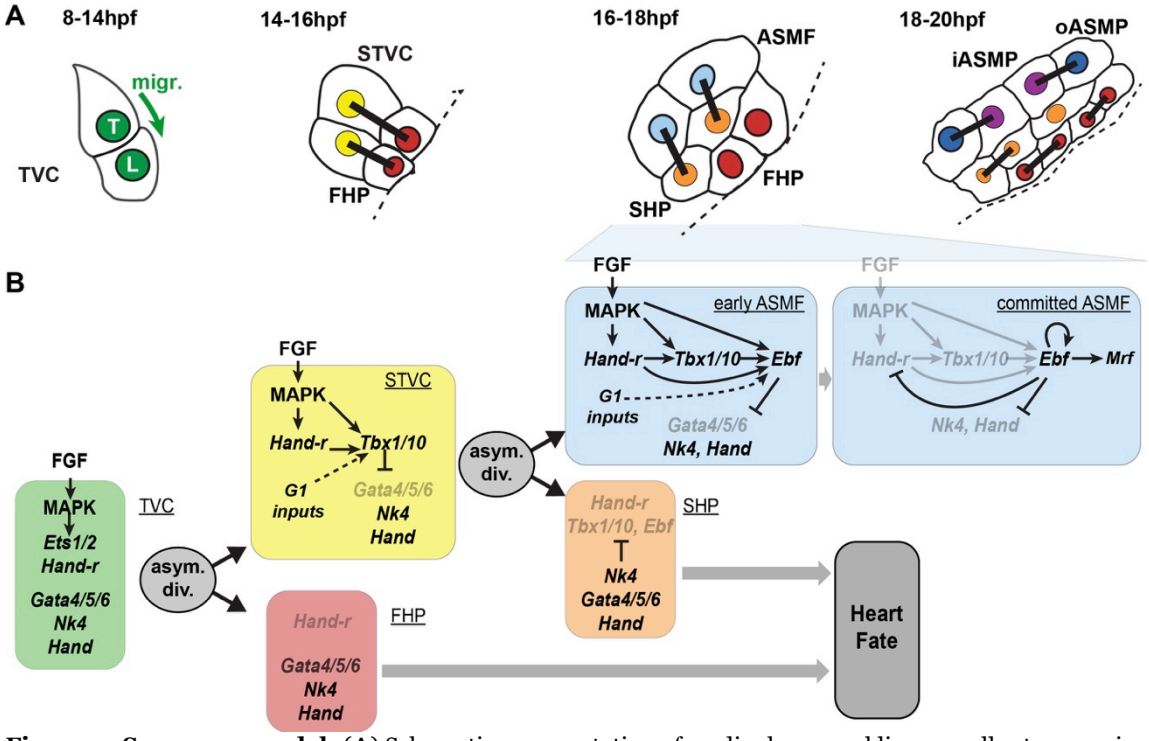

Figure 7. Summary model. (**A**) Schematic representation of cardiopharyngeal lineage cells at successive time points representing the main fate transitions. hpf: hours post-fertilization; TVC: trunk ventral cells; L: Leader T: trailer; migr.: migration; STVC: second trunk ventral cells; FHP: first heart precursors; dotted line: midline; black bars link sister cells; ASMF: atrial siphon muscle founder cells; SHP: second heart precursors; iASMP: inner atrial siphon muscle precursors; oASMP: outer atrial siphon muscle precursor (these cells correspond to stem-cell-like *Mrf*-; Notch+ precursors and *Mrf*+; Notch- differentiating myoblasts, respectively; see (Razy-Krajka et al., 2014) for details). (**B**) Lineage diagram and documented regulatory relationships between indicated genes and pathways, as showing here and in (Razy-Krajka et al., 2014; Wang et al., 2013). In TVCs, primed heart and ASM markers are coexpressed, and maintenance of the STVC and ASM markers requires ongoing FGF/MAPK signaling. Following the first oriented and asymmetric cell division, FGF-MAPK is maintained only in the STVCs, which permits the continued expression of Hand-r and the activation of *Tbx1/10*. Cell division, presumably through G1-specific inputs, contributes to *Tbx1/10* activation, and Tbx1/10 function antagonizes *Gata4/5/6* expression (Wang et al., 2013). In the FHPs, termination of FGF-MAPK signaling inhibits *Hand-r* expression and prevents *Tbx1/10* activation. Following oriented and asymmetric division of the STVCs, FGF/MAPK signaling persists only in the ASMFs, where it permits the transient maintenance of *Hand-r* and *Tbx1/10*, both of which act in parallel to FGF/MAPK to activate *Ebf* expression, together with contributions from presumed G1 inputs. Ebf activities further antagonize the cardiac program (marked by *Gata4/5/6*, *Nk4/Nkx2.5* and *Hand* expression; (Razy-Krajka et al., 2014; Stolfi et al., 2010; Wang et al., 2013)). Once Ebf expression reaches "high levels", its regulation becomes MAPK-independent and self-activating (this study). It also feeds back negatively on early activators such as Hand-r, and promotes the expression of the muscle determinant *Mrf* (Razy-Krajka et al., 2014; Tolkin and Christiaen, 2016). We propose that this transition represents commitment to an ASM fate. In the SHPs, termination of FGF/MAPK signaling prevents maintenance of Hand-r and Tbx1/10 expression, which, together with repressive inputs from Nk4/Nkx2.5, inhibits *Ebf* activation (Wang et al., 2013), and permits heart fate specification (Wang et al., submitted).

bioRxiv preprint doi: https://doi.org/10.1101/138701; this version posted January 12, 2018. The copyright holder for this preprint (which was not certified by peer review) is the author/funder. All rights reserved. No reuse allowed without permission.

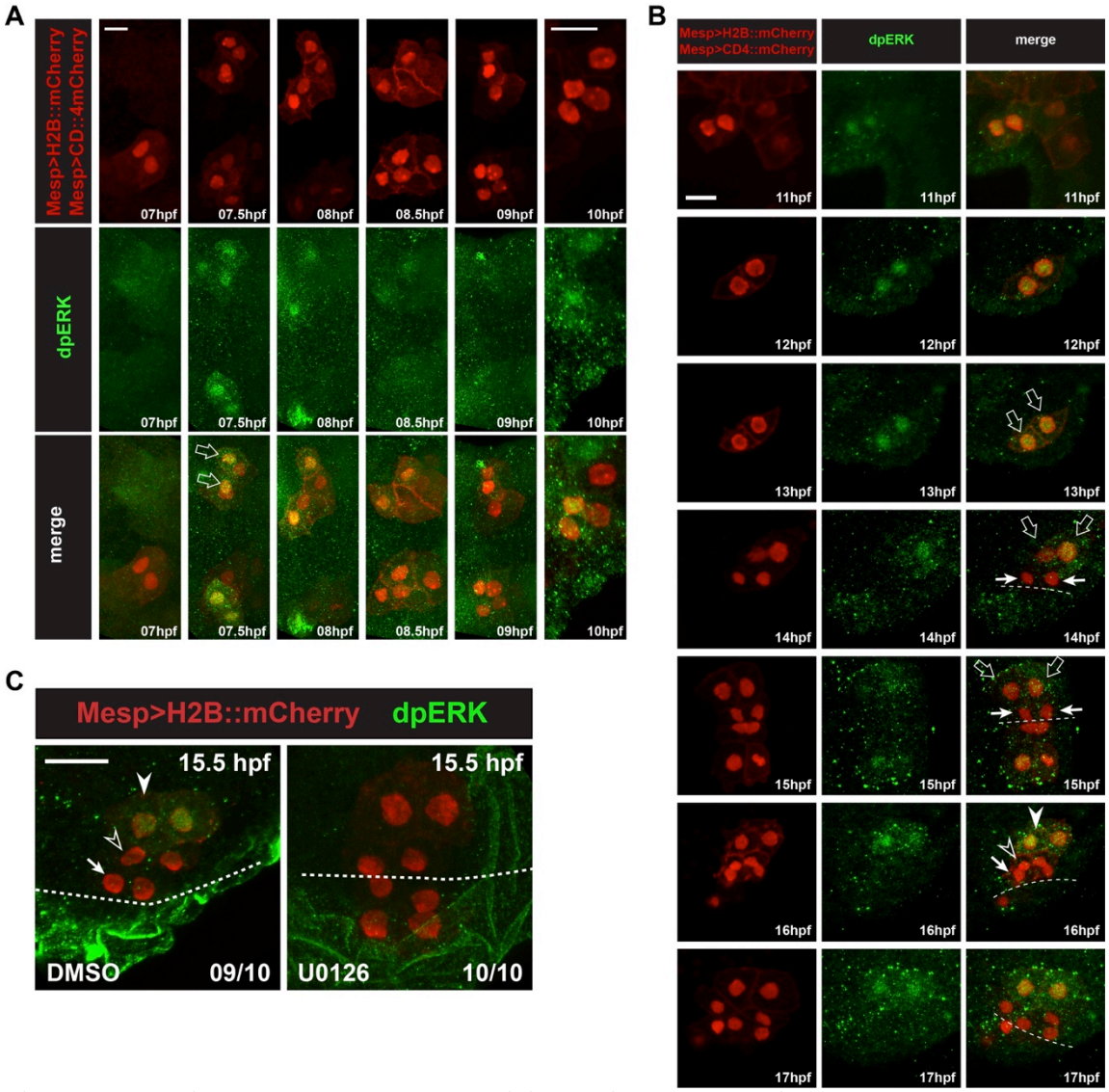

Figure S1. Detailed patterns of MAPK activity during early cardiopharyngeal development. (**A**) MAPK activation during TVC induction. Close-up views of B7.5 lineage cells marked with Mesp>H2B::mCherry (nuclei) and Mesp>hCD4::mCherry (membranes) and immunostained for dpERK at indicated successive time points between 7 and 10hpf. DpERK staining was not detected in the founder cells at 7hpf, but increased sharply and specifically in the smaller trunk ventral cells (TVCs, open arrows) at 7.5hpf, but not in the larger anterior tail muscles (ATMs). DpERK staining persisted throughout TVC migration (see also B). (B) MAPK activation patterns during cardiopharyngeal fate diversification. DpERK staining was clearly detected in migrating TVCs (open arrows, 11 to 13hpf); in lateral large STVCs (open arrows, 14 to 15hpf), but not in the small median first heart precursors (FHPs, arrows, 14 to 15hpf); in the large lateral atrial siphon muscle founder cells (ASMFs, solid arrowheads, 16 to 17hpf), but neither in the FHPs (arrows), nor in the second heart precursors (SHPs, open arrowheads). (**C**) Treatment with the MEK inhibitor U0126 from 12 to 15.5hpf abolished dpERK staining in the lateral STVCs, compared to a control treatment with DMSO. Numbers of embryos showing the presented pattern out of the total numbers of embryos are shown.

bioRxiv preprint doi: https://doi.org/10.1101/138701; this version posted January 12, 2018. The copyright holder for this preprint (which was not certified by peer review) is the author/funder. All rights reserved. No reuse allowed without permission.

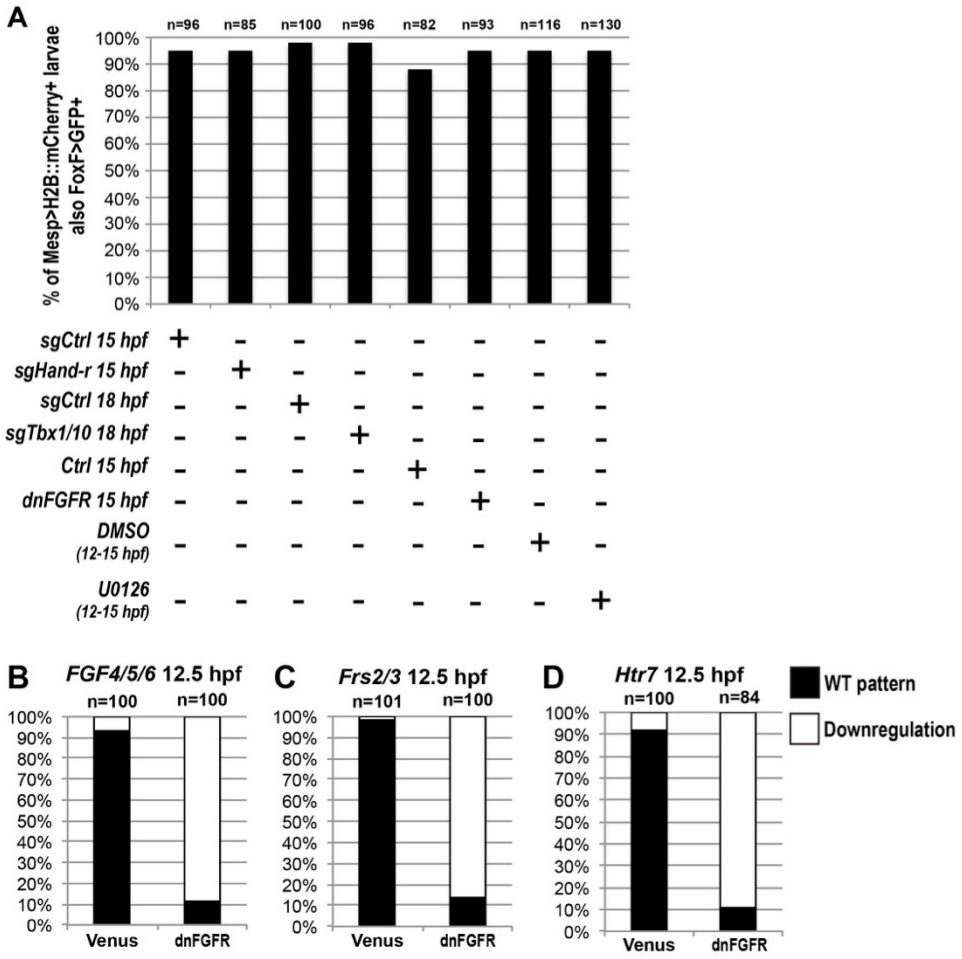

Figure S2 - part 1.

(A) Effects of perturbations on *Foxf* TVC-specific enhancer activity. Proportions of Mesp>H2B:mCherry-positive embryos showing Foxf::bpFog-1>NLS:GFP activity (i.e. GFP+) in the indicated conditions : TVC-specific CRISPR/Cas9 mediated loss-of-function of Hand-r (sgHand-r), and corresponding control (Neurogenin/sgCtrl) at 15 hpf ; TVC-specific CRISPR/Cas9 mediated loss-of-function of Tbx1/10 (sgTbx1/10) and corresponding control (Neurogenin/sgCtrl) at 18 hpf ; TVC-targeted dnFGFR embryos (FoxF::bpFog-1>dnFGFR) and corresponding control (FoxF::bpFog-1>NLS::LacZ) at 15 hpf ; Inhibition of MAPK activity with 4-hour incubations in U0126 (DMSO as vehicle control) at indicated times. TVCS and their progeny marked with Mesp>H2B::mCherry and possible effects on *Foxf* enhancer activity of these perturbations have been verified with TVC-specific green staining. There were no significant difference in the proportions of GFP+ embryos between each perturbations and controls. **(B-D) Other markers expressed in the TVC need continuous FGF-MAPK inputs for maintenance**. All panels show the proportions of 12.5hpf embryos halves showing expression of the indicated genes in late TVCs, following electroporation of either a Foxf(TVC)>Venus control of a Foxf(TVC)>dnFGFR construct that inhibits signaling through FGFR. Wild-type pattern were first reported in (Razy-Krajka et al., 2014).

bioRxiv preprint doi: https://doi.org/10.1101/138701; this version posted January 12, 2018. The copyright holder for this preprint (which was not certified by peer review) is the author/funder. All rights reserved. No reuse allowed without permission.

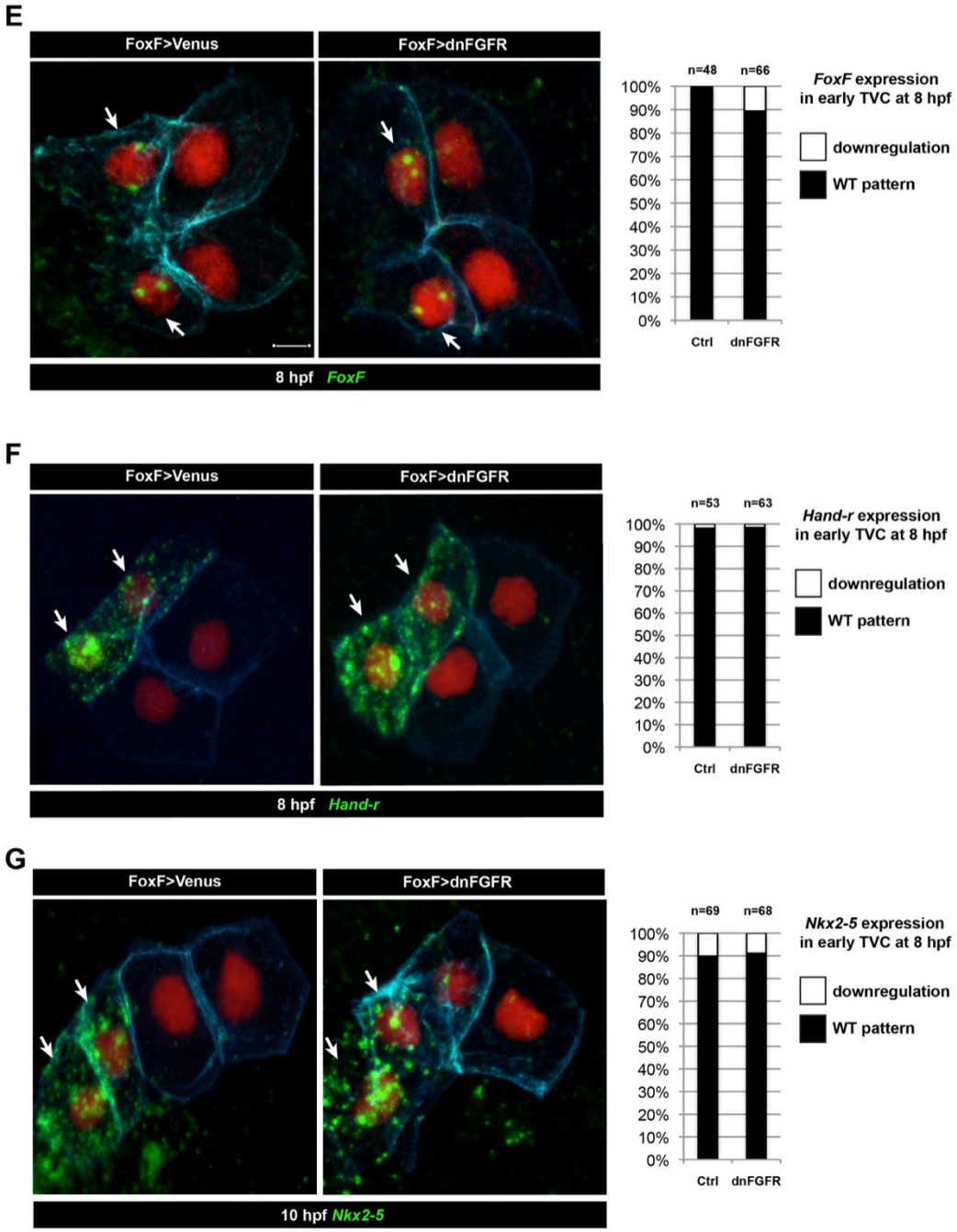

Figure S2 - part 2.
(E-G) Foxf>dnFGFR does not inhibit TVC induction. TVC-specific expression of dnFGFR (FoxF::bpFog-1>dnFGFR) do not show difference in TVC markers expression in comparison to control (FoxF::bpFog-1>Venus) in early TVC (*Foxf* and *Hand-r* at 8 hpf, *Nkx2-5* at 10 hpf).
Arrows indicate anterior TVCs, adjacent cells on the right are ATMs, which do not express TVC markers.

bioRxiv preprint doi: https://doi.org/10.1101/138701; this version posted January 12, 2018. The copyright holder for this preprint (which was not certified by peer review) is the author/funder. All rights reserved. No reuse allowed without permission.

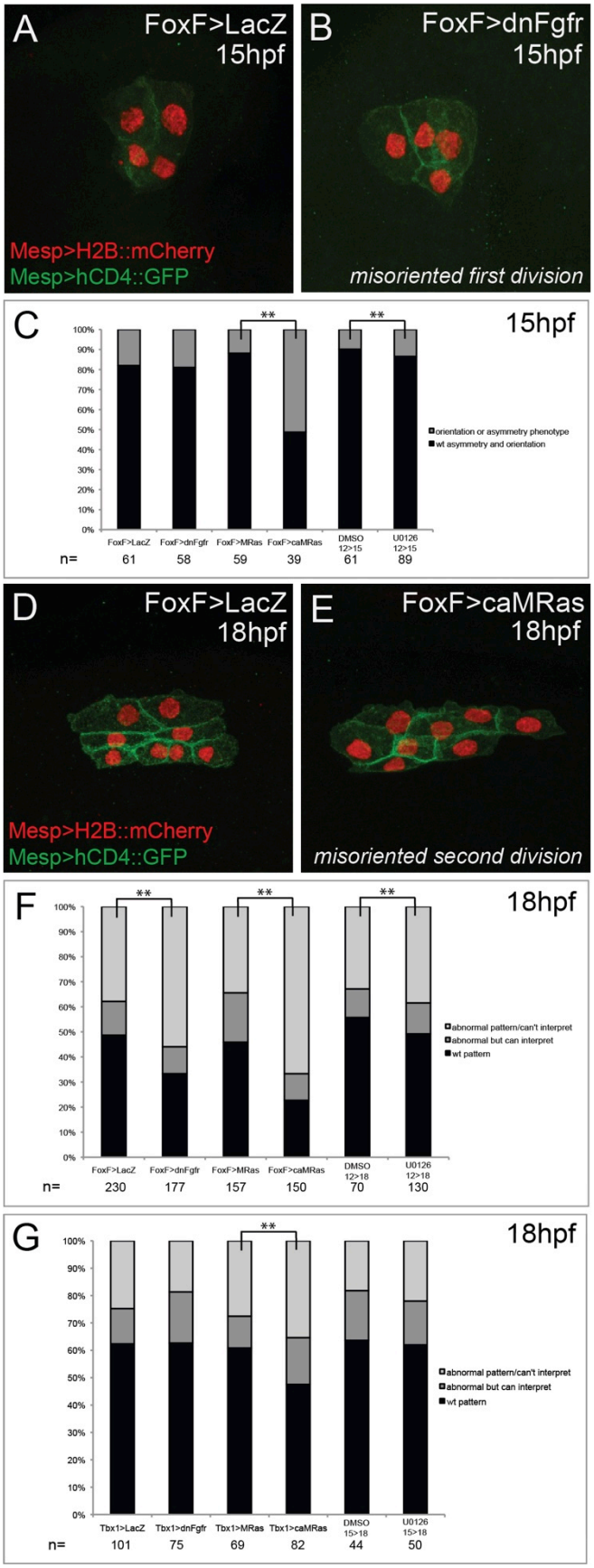

Figure S3. Effects of defined FGF-MAPK signaling perturbations on cell division patterns in the cardiopharyngeal lineage. **(A)** Representative phenotype in unperturbed conditions (control plasmid: *Foxf>LacZ*) at 15hpf. TVCs divide asymmetrically and in a medio-lateral orientation. **(B)** Representative misoriented TVC division phenotype (Foxf>dnFGFR). One TVC divided improperly in the antero-posterior axis. **(C)** Proportions of embryo halves showing wild-type vs. orientation or symmetry phenotype, scored at 15hpf. For pharmacological treatments, embryos were incubated in DMSO or U0126 from 12hpf-15hpf. Proportions differ significantly between *Foxf>MRas* and *Foxf>caMRas*, and between DMSO and U0126 treatment conditions (** indicates p-value<0.01, Chi^2 test). **(D)** Representative phenotype in unperturbed conditions (FoxF>LacZ) at 18hpf. STVCs divide in a medio-lateral orientation. **(E)** Representative misoriented STVC division phenotype (FoxF>caMRas), scored as 'abnormal but can interpret.' STVCs likely divided improperly in the antero-posterior axis. **(F)** Proportions of larva halves in *Foxf*(TVC)-driven perturbations showing wild-type pattern vs. orientation and/or symmetry phenotypes, patterns scored at 18hpf as abnormal but interpretable or abnormal/can't interpret. For pharmacological treatments, larvae were incubated in DMSO or U0126 from 12hpf-18hpf. Proportions differ significantly in all conditions in comparison to the corresponding control (** indicates p-value<0.01, Chi^2 test). **(G)** Proportions of larva halves in *Tbx1*-driven perturbations showing wild-type pattern vs. orientation and/or symmetry phenotype, patterns scored at 18hpf as abnormal but interpretable or abnormal/can't interpret. For pharmacological treatments, larvae were incubated in DMSO or U0126 from 15hpf-18hpf. Proportions differ significantly only between Tbx1>MRas and Tbx1>caMRas conditions (** indicates p-value<0.01, Chi^2 test).

bioRxiv preprint doi: https://doi.org/10.1101/138701; this version posted January 12, 2018. The copyright holder for this preprint (which was not certified by peer review) is the author/funder. All rights reserved. No reuse allowed without permission.

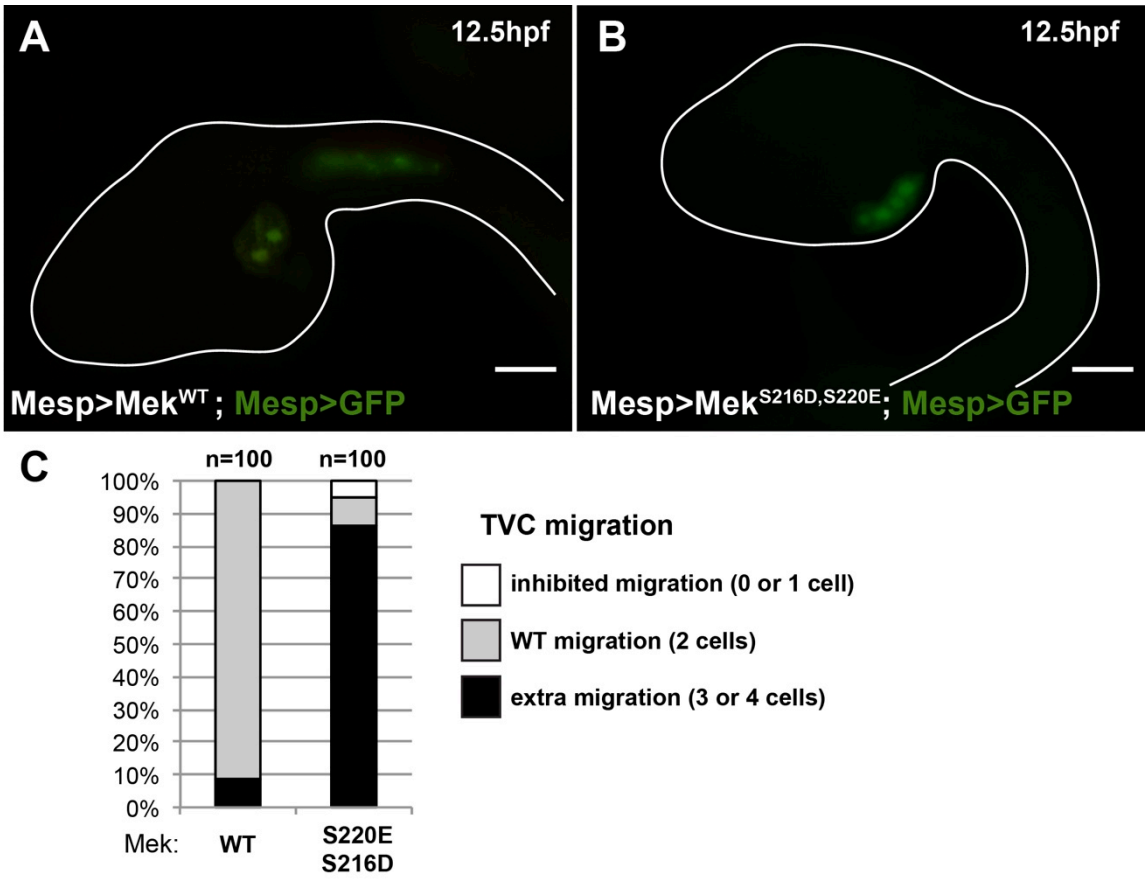

Figure S4. The constitutively active MEK^{S216D,S220E} mutant is sufficient to impose a TVC identity to the whole B7.5 lineage. (A) Control late tailbud embryo showing the left side B7.5 lineage expressing GFP and a MEK^{WT} control under the control of the *Mesp* enhancer. Two TVCs and two ATMs are normally induced, and TVCs migrated into the trunk. (B) Late tailbud embryo showing the left side B7.5 lineage expressing GFP and a MEK^{S216D,S220E} mutant under the control of the *Mesp* enhancer. Four cells are observed as having migrated into the trunk, indicating that they have been induced to acquire a TVC fate and migrate, replicating FGF-MAPK gain-of-function phenotypes as described in (Davidson et al., 2006). (C) Proportions of embryo halves showing the indicated phenotypes. Extra migration is interpreted as ectopic induction of the TVC fate in all B7.5 lineage cells. Scale bar ~ 20μm.

bioRxiv preprint doi: https://doi.org/10.1101/138701; this version posted January 12, 2018. The copyright holder for this preprint (which was not certified by peer review) is the author/funder. All rights reserved. No reuse allowed without permission.

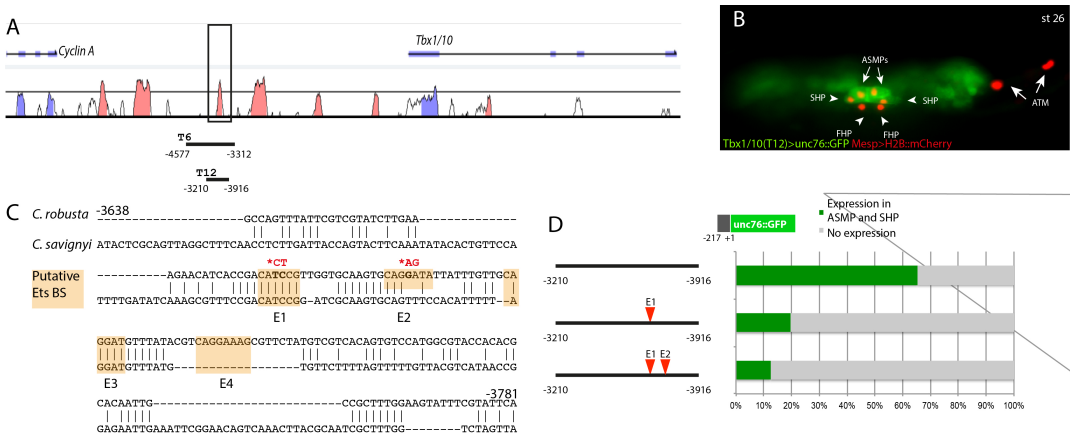

Figure S5. The Tbx1/10 enhancer has conserved putative Ets binding sites required for reporter gene expression. (A) Alignment of *Tbx1/10* locus between *Ciona robusta/Ciona savignyi* using VISTA. (B) *Ciona* larva (st 26) expressing GFP driven by the *T12* element, a STVC-specific *Tbx1/10* enhancer (green) and Mesp>H2B::mCherry to track the B7.5 lineage cell nuclei (red). The *Tbx1/10* enhancer drives the unc76::GFP reporter in the STVC progeny, including ASM precursors (ASMPs) (white arrows) and the second heart precursors (SHPs) (white arrowheads). No expression is detected in the first heart precursors (FHPs) (white arrowheads) and anterior tail muscle (ATMs) (orange arrows). (C) Sequence alignment of *Tbx1/10* enhancer between *Ciona robusta/Ciona savignyi* Conserved blocks in the orange boxes with putative Ets binding sites. (D) Proportion of larvae expressing both GFP and mCherry in the STVC progeny when co-electroporated wild-type and mutant *Tbx1/10* reporters lacking the indicated putative Ets binding sites and Mesp>H2B::mCherry in comparison to the control (no enhancer, only *Tbx1/10* basal promoter driving unc::76GFP). n: number of electroporated larval halves.

bioRxiv preprint doi: https://doi.org/10.1101/138701; this version posted January 12, 2018. The copyright holder for this preprint (which was not certified by peer review) is the author/funder. All rights reserved. No reuse allowed without permission.

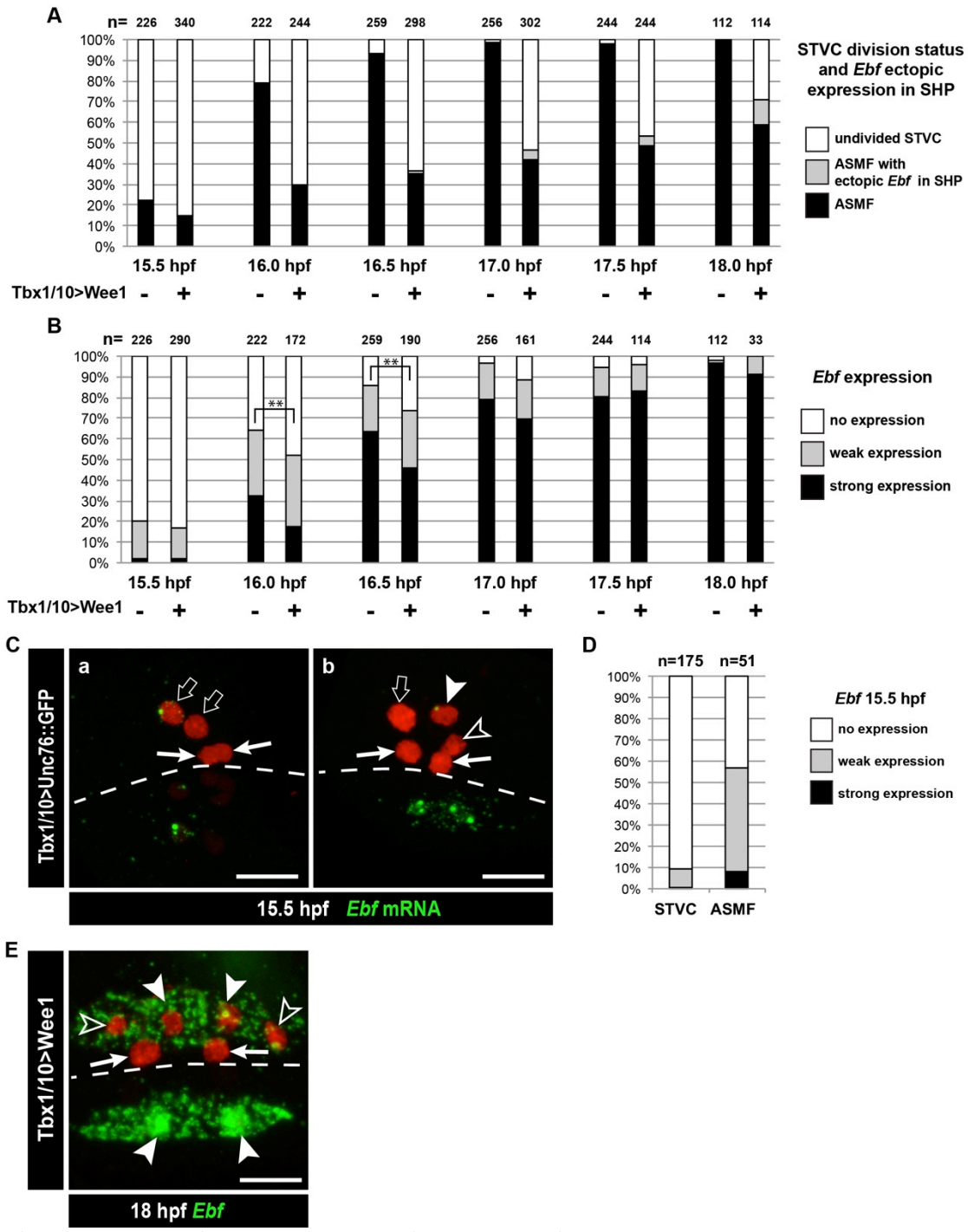

Figure S6. Dynamics of Ebf upregulation and entrainment by the cell cycle. (**A**) Proportions of larva halves fixed at successive time points and showing undivided STVCs, or ASMFs with or without ectopic *Ebf* expression in the SHPs following STVC-specific expression of the G2/M inhibitor Wee1 (+), or a control construct (-). See Figure S6E for an example of ectopic *Ebf* expression in the SHPs (grey labels). Note the sharp increase in % of larva with ASMF nbetween 15.5 and 16hpf, indicating that mitosis occurs primarily during this time window, but is delayed in a majority of larvae upon Wee1 misexpression. (**B**) Proportions of larva halves with cells showing indicated Ebf expression. The numbers (n) for cells expressing Wee1 focus on cells that have not divided (% shown in E), to estimate the dynamics of *Ebf* activation in G2/M-inhibited cells. Control cells consist mostly ASMFs after 15.5hpf as shown in (E). Wee1 and controls distributions differ significantly only at 16 and 16.5hpf (**, $p<0.01$, Chi^2 test), suggesting that Wee1 merely delays the accumulation of Ebf transcripts. (**A**) 15.5hpf Cardiopharyngeal lineage cells

bioRxiv preprint doi: https://doi.org/10.1101/138701; this version posted January 12, 2018. The copyright holder for this preprint (which was not certified by peer review) is the author/funder. All rights reserved. No reuse allowed without permission.

expressing Mesp>H2B::mCherry (red) and control Tbx1/10>unc76::GFP construct (not visible). **Rare precocious activation of *Ebf* transcription in STVCs.** (**C.a**) Green nuclear dot indicates nascent Ebf transcription in an STVC (open arrow), but not the other, and not in the first heart precursors (FHP; arrow). (**C.b**) left pair of nuclei shows an STVC (open arrow) and an FHP (arrow), neither of which express *Ebf*, whereas the cousin ASMF (solid arrowhead) shows nascent *Ebf* transcription (green dot). Dotted line : midline. (**D**) Proportions of STVCs and ASMFs showing indicated *Ebf* expression patterns. Note that >90% of STVCs do not express *Ebf*, which turns on almost exclusively in ASMFs. (**E**) Cardiopharyngeal lineage cells with *Ebf* expression in the ASMFs (solid arrowheads), and ectopically in the SHP (open arrowheads), but not in the FHPs (arrows), following misexpression of Wee1 using the STVC-specific *Tbx1/10 T12* enhancer. Dotted line: midline.

bioRxiv preprint doi: https://doi.org/10.1101/138701; this version posted January 12, 2018. The copyright holder for this preprint (which was not certified by peer review) is the author/funder. All rights reserved. No reuse allowed without permission.

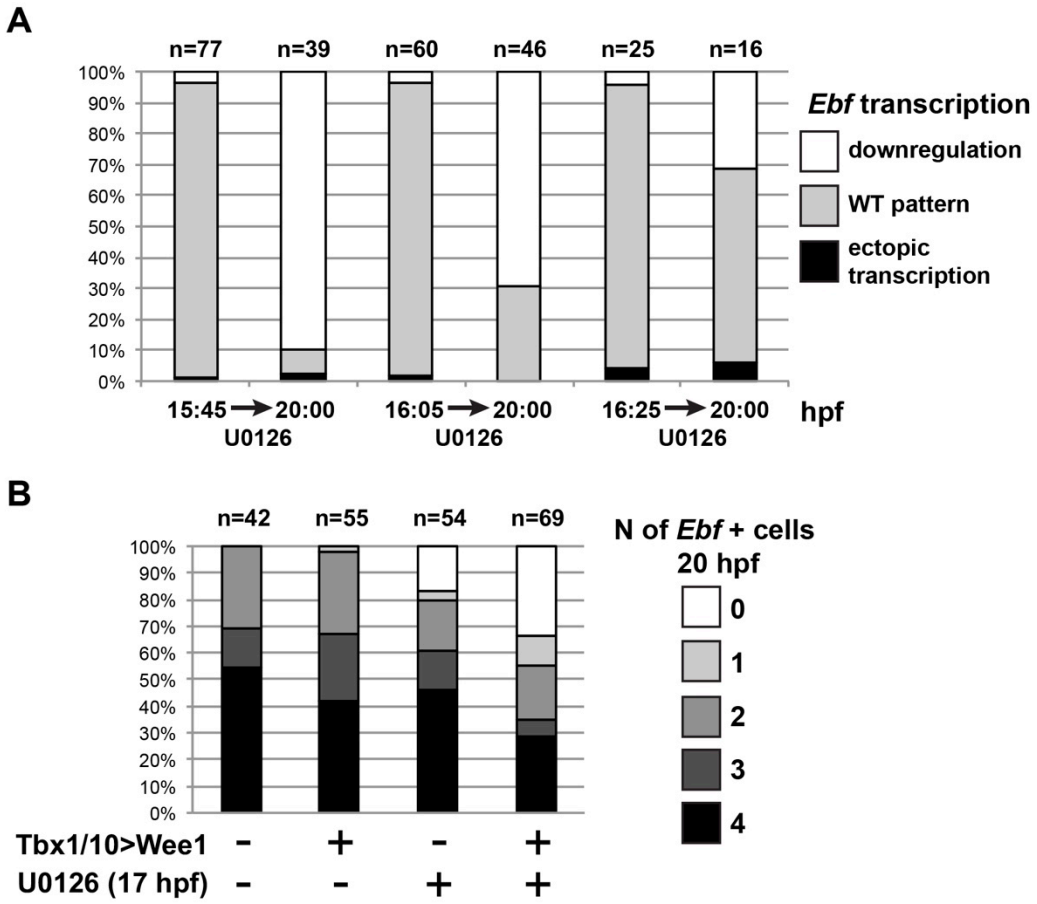

Figure S7. MAPK signaling is necessary for *Ebf* expression only in early ASMF, and cell cycle inputs shorten the MAPK-dependent period. (**A**) Proportions of larva halves showing the indicated *Ebf* transcriptional activity (assayed using intronic probes). Batches of larvae expressing *Mesp>H2B::mCherry* were split to be fixed for WMFISH or treated with U0126 at 3 successive time points (15.75hpf, 16hpf or 16.25hpf), and the treated larvae were fixed at 20hpf. This data shows that, although all batches expressed *Ebf* at the beginning of the experiment, only when MEK was inhibited later (16.25hpf) did *Ebf* transcription persist in 20hpf larvae. (**B**) Proportions of larva halves showing the indicated numbers of *Ebf*+ cells at 20hpf, following expression of the G2/M inhibitor Wee1 in the STVCs, under the control of the *Tbx1/10 T12* enhancer (+). Negative controls (-) were electroporated with a *Tbx1/10(T12)>Venus* construct. Larvae were also treated with U0126 (+) or DMSO (as negative control, (-)), starting at 17hpf, which corresponds to the transition from a MAPK-dependent to a MAPK-independent autoregulative mode of *Ebf* expression (see Figure 6A). Wee1-induced delays in cell cycle progression increased the sensitivity of late *Ebf* expression to MAPK inhibition, further supporting the notion that cell divisions accelerate the transition from MAPK-dependent to MAPK-independent self-activating regulation of *Ebf* transcription.

bioRxiv preprint doi: https://doi.org/10.1101/138701; this version posted January 12, 2018. The copyright holder for this preprint (which was not certified by peer review) is the author/funder. All rights reserved. No reuse allowed without permission.

REFERENCES

Abu-Issa, R., Smyth, G., Smoak, I., Yamamura, K., Meyers, E.N., 2002. Fgf8 is required for pharyngeal arch and cardiovascular development in the mouse. Development 129, 4613-4625.

Aggarwal, V.S., Liao, J., Bondarev, A., Schimmang, T., Lewandoski, M., Locker, J., Shanske, A., Campione, M., Morrow, B.E., 2006. Dissection of Tbx1 and Fgf interactions in mouse models of 22q11DS suggests functional redundancy. Human molecular genetics 15, 3219-3228.

Alsan, B.H., Schultheiss, T.M., 2002. Regulation of avian cardiogenesis by Fgf8 signaling. Development 129, 1935-1943.

Barron, M., Gao, M., Lough, J., 2000. Requirement for BMP and FGF signaling during cardiogenic induction in non-precardiac mesoderm is specific, transient, and cooperative. Developmental dynamics : an official publication of the American Association of Anatomists 218, 383-393.

Beh, J., Shi, W., Levine, M., Davidson, B., Christiaen, L., 2007. FoxF is essential for FGF-induced migration of heart progenitor cells in the ascidian Ciona intestinalis. Development 134, 3297-3305.

Bertrand, V., Hudson, C., Caillol, D., Popovici, C., Lemaire, P., 2003. Neural tissue in ascidian embryos is induced by FGF9/16/20, acting via a combination of maternal GATA and Ets transcription factors. Cell 115, 615-627.

Bondue, A., Lapouge, G., Paulissen, C., Semeraro, C., Iacovino, M., Kyba, M., Blanpain, C., 2008. Mesp1 acts as a master regulator of multipotent cardiovascular progenitor specification. Cell stem cell 3, 69-84.

Bothe, I., Tenin, G., Oseni, A., Dietrich, S., 2011. Dynamic control of head mesoderm patterning. Development 138, 2807-2821.

Brand, T., 2003. Heart development: molecular insights into cardiac specification and early morphogenesis. Developmental biology 258, 1-19.

Brown, C.B., Wenning, J.M., Lu, M.M., Epstein, D.J., Meyers, E.N., Epstein, J.A., 2004. Cre-mediated excision of Fgf8 in the Tbx1 expression domain reveals a critical role for Fgf8 in cardiovascular development in the mouse. Developmental biology 267, 190-202.

Buckingham, M., Vincent, S.D., 2009. Distinct and dynamic myogenic populations in the vertebrate embryo. Current opinion in genetics & development 19, 444-453.

Cai, C.L., Liang, X., Shi, Y., Chu, P.H., Pfaff, S.L., Chen, J., Evans, S., 2003. Isl1 identifies a cardiac progenitor population that proliferates prior to differentiation and contributes a majority of cells to the heart. Developmental cell 5, 877-889.

Chan, S.S., Hagen, H.R., Swanson, S.A., Stewart, R., Boll, K.A., Aho, J., Thomson, J.A., Kyba, M., 2016. Development of Bipotent Cardiac/Skeletal Myogenic Progenitors from MESP1+ Mesoderm. Stem cell reports 6, 26-34.

bioRxiv preprint doi: https://doi.org/10.1101/138701; this version posted January 12, 2018. The copyright holder for this preprint (which was not certified by peer review) is the author/funder. All rights reserved. No reuse allowed without permission.

1168 Chan, S.S., Shi, X., Toyama, A., Arpke, R.W., Dandapat, A., Iacovino, M., Kang, J.,
1169 Le, G., Hagen, H.R., Garry, D.J., Kyba, M., 2013. Mesp1 patterns mesoderm into
1170 cardiac, hematopoietic, or skeletal myogenic progenitors in a context-dependent
1171 manner. Cell stem cell 12, 587-601.

1172 Chen, L., Fulcoli, F.G., Tang, S., Baldini, A., 2009. Tbx1 regulates proliferation and
1173 differentiation of multipotent heart progenitors. Circulation research 105, 842-851.

1174 Choi, C.Y., Lee, Y.M., Kim, Y.H., Park, T., Jeon, B.H., Schulz, R.A., Kim, Y., 1999. The
1175 homeodomain transcription factor NK-4 acts as either a transcriptional activator or
1176 repressor and interacts with the p300 coactivator and the Groucho corepressor. The
1177 Journal of biological chemistry 274, 31543-31552.

1178 Christiaen, L., Davidson, B., Kawashima, T., Powell, W., Nolla, H., Vranizan, K.,
1179 Levine, M., 2008. The transcription/migration interface in heart precursors of Ciona
1180 intestinalis. Science 320, 1349-1352.

1181 Christiaen, L., Wagner, E., Shi, W., Levine, M., 2009a. Electroporation of transgenic
1182 DNAs in the sea squirt Ciona. Cold Spring Harbor protocols 2009, pdb prot5345.

1183 Christiaen, L., Wagner, E., Shi, W., Levine, M., 2009b. Isolation of sea squirt (Ciona)
1184 gametes, fertilization, dechorionation, and development. Cold Spring Harbor protocols
1185 2009, pdb prot5344.

1186 Christiaen, L., Wagner, E., Shi, W., Levine, M., 2009c. Whole-mount in situ
1187 hybridization on sea squirt (Ciona intestinalis) embryos. Cold Spring Harbor protocols
1188 2009, pdb prot5348.

1189 Cinnamon, E., Helman, A., Ben-Haroush Schyr, R., Orian, A., Jimenez, G., Paroush,
1190 Z., 2008. Multiple RTK pathways downregulate Groucho-mediated repression in
1191 Drosophila embryogenesis. Development 135, 829-837.

1192 Cinnamon, E., Paroush, Z., 2008. Context-dependent regulation of Groucho/TLE-
1193 mediated repression. Current opinion in genetics & development 18, 435-440.

1194 Cooley, J., Whitaker, S., Sweeney, S., Fraser, S., Davidson, B., 2011. Cytoskeletal
1195 polarity mediates localized induction of the heart progenitor lineage. Nature cell biology
1196 13, 952-957.

1197 Cota, C.D., Davidson, B., 2015. Mitotic Membrane Turnover Coordinates Differential
1198 Induction of the Heart Progenitor Lineage. Developmental cell 34, 505-519.

1199 Cowley, S., Paterson, H., Kemp, P., Marshall, C.J., 1994. Activation of MAP kinase
1200 kinase is necessary and sufficient for PC12 differentiation and for transformation of
1201 NIH 3T3 cells. Cell 77, 841-852.

1202 Dalton, S., 2015. Linking the Cell Cycle to Cell Fate Decisions. Trends in cell biology
1203 25, 592-600.

1204 Davidson, B., 2007. Ciona intestinalis as a model for cardiac development. Seminars
1205 in cell & developmental biology 18, 16-26.

bioRxiv preprint doi: https://doi.org/10.1101/138701; this version posted January 12, 2018. The copyright holder for this preprint (which was not certified by peer review) is the author/funder. All rights reserved. No reuse allowed without permission.

1206 Davidson, B., Levine, M., 2003. Evolutionary origins of the vertebrate heart:
1207 Specification of the cardiac lineage in Ciona intestinalis. Proceedings of the National
1208 Academy of Sciences of the United States of America 100, 11469-11473.

1209 Davidson, B., Shi, W., Beh, J., Christiaen, L., Levine, M., 2006. FGF signaling
1210 delineates the cardiac progenitor field in the simple chordate, Ciona intestinalis. Genes
1211 & development 20, 2728-2738.

1212 Davidson, B., Shi, W., Levine, M., 2005. Uncoupling heart cell specification and
1213 migration in the simple chordate Ciona intestinalis. Development 132, 4811-4818.

1214 de Pater, E., Clijsters, L., Marques, S.R., Lin, Y.-F., Garavito-Aguilar, Z.V., Yelon, D.,
1215 Bakkers, J., 2009. Distinct phases of cardiomyocyte differentiation regulate growth of
1216 the zebrafish heart. Development 136, 1633-1641.

1217 Delsuc, F., Brinkmann, H., Chourrout, D., Philippe, H., 2006. Tunicates and not
1218 cephalochordates are the closest living relatives of vertebrates. Nature 439, 965-968.

1219 Diogo, R., Kelly, R.G., Christiaen, L., Levine, M., Ziermann, J.M., Molnar, J.L.,
1220 Noden, D.M., Tzahor, E., 2015a. The Cardiopharyngeal Field and Vertebrate Evolution:
1221 A New Heart for a New Head. Nature in press.

1222 Diogo, R., Kelly, R.G., Christiaen, L., Levine, M., Ziermann, J.M., Molnar, J.L.,
1223 Noden, D.M., Tzahor, E., 2015b. A new heart for a new head in vertebrate
1224 cardiopharyngeal evolution. Nature 520, 466-473.

1225 Dumollard, R., Minc, N., Salez, G., Aicha, S.B., Bekkouche, F., Hebras, C.,
1226 Besnardeau, L., McDougall, A., 2017. The invariant cleavage pattern displayed by
1227 ascidian embryos depends on spindle positioning along the cell's longest axis in the
1228 apical plane and relies on asynchronous cell divisions. eLife 6.

1229 Farley, E.K., Olson, K.M., Zhang, W., Brandt, A.J., Rokhsar, D.S., Levine, M.S., 2015.
1230 Suboptimization of developmental enhancers. Science 350, 325-328.

1231 Farley, E.K., Olson, K.M., Zhang, W., Rokhsar, D.S., Levine, M.S., 2016. Syntax
1232 compensates for poor binding sites to encode tissue specificity of developmental
1233 enhancers. Proceedings of the National Academy of Sciences of the United States of
1234 America 113, 6508-6513.

1235 Frazer, K.A., Pachter, L., Poliakov, A., Rubin, E.M., Dubchak, I., 2004. VISTA:
1236 computational tools for comparative genomics. Nucleic acids research 32, W273-279.

1237 Gainous, T.B., Wagner, E., Levine, M., 2015. Diverse ETS transcription factors
1238 mediate FGF signaling in the Ciona anterior neural plate. Developmental biology 399,
1239 218-225.

1240 Gandhi, S., Haeussler, M., Razy-Krajka, F., Christiaen, L., Stolfi, A., 2017a.
1241 Evaluation and rational design of guide RNAs for efficient CRISPR/Cas9-mediated
1242 mutagenesis in Ciona. Developmental biology.

bioRxiv preprint doi: https://doi.org/10.1101/138701; this version posted January 12, 2018. The copyright holder for this preprint (which was not certified by peer review) is the author/funder. All rights reserved. No reuse allowed without permission.

1243 Gandhi, S., Haeussler, M., Razy-Krajka, F., Christiaen, L., Stolfi, A., 2017b.
1244 Evaluation and rational design of guide RNAs for efficient CRISPR/Cas9-mediated
1245 mutagenesis in Ciona. bioRxiv.

1246 George, V., Colombo, S., Targoff, K.L., 2015. An early requirement for nkx2.5 ensures
1247 the first and second heart field ventricular identity and cardiac function into adulthood.
1248 Developmental biology 400, 10-22.

1249 Gopalakrishnan, S., Comai, G., Sambasivan, R., Francou, A., Kelly, R.G., Tajbakhsh,
1250 S., 2015. A Cranial Mesoderm Origin for Esophagus Striated Muscles. Developmental
1251 cell 34, 694-704.

1252 Gotoh, N., Laks, S., Nakashima, M., Lax, I., Schlessinger, J., 2004. FRS2 family
1253 docking proteins with overlapping roles in activation of MAP kinase have distinct
1254 spatial-temporal patterns of expression of their transcripts. FEBS letters 564, 14-18.

1255 Gueroult-Bellone, M., Nitta, K.R., Kari, W., Jacox, E., Beule Dauzat, R., Vincentelli,
1256 R., Diarra, C., Rothbacher, U., Dantec, C., Cambillau, C., Piette, J., Lemaire, P., 2017.
1257 Spacer sequences separating transcription factor binding motifs set enhancer quality
1258 and strength. bioRxiv.

1259 Hasson, P., Egoz, N., Winkler, C., Volohonsky, G., Jia, S., Dinur, T., Volk, T., Courey,
1260 A.J., Paroush, Z., 2005. EGFR signaling attenuates Groucho-dependent repression to
1261 antagonize Notch transcriptional output. Nature genetics 37, 101-105.

1262 Haupaix, N., Abitua, P.B., Sirour, C., Yasuo, H., Levine, M., Hudson, C., 2014.
1263 Ephrin-mediated restriction of ERK1/2 activity delimits the number of pigment cells in
1264 the Ciona CNS. Developmental biology 394, 170-180.

1265 Hotta, K., Mitsuhara, K., Takahashi, H., Inaba, K., Oka, K., Gojobori, T., Ikeo, K.,
1266 2007. A web-based interactive developmental table for the ascidian Ciona intestinalis,
1267 including 3D real-image embryo reconstructions: I. From fertilized egg to hatching
1268 larva. Developmental dynamics : an official publication of the American Association of
1269 Anatomists 236, 1790-1805.

1270 Hu, T., Yamagishi, H., Maeda, J., McAnally, J., Yamagishi, C., Srivastava, D., 2004.
1271 Tbx1 regulates fibroblast growth factors in the anterior heart field through a reinforcing
1272 autoregulatory loop involving forkhead transcription factors. Development 131, 5491-
1273 5502.

1274 Hudson, C., Darras, S., Caillol, D., Yasuo, H., Lemaire, P., 2003. A conserved role for
1275 the MEK signalling pathway in neural tissue specification and posteriorisation in the
1276 invertebrate chordate, the ascidian Ciona intestinalis. Development 130, 147-159.

1277 Hutson, M.R., Zeng, X.L., Kim, A.J., Antoon, E., Harward, S., Kirby, M.L., 2010.
1278 Arterial pole progenitors interpret opposing FGF/BMP signals to proliferate or
1279 differentiate. Development 137, 3001-3011.

1280 Ilagan, R., Abu-Issa, R., Brown, D., Yang, Y.P., Jiao, K., Schwartz, R.J., Klingensmith,
1281 J., Meyers, E.N., 2006. Fgf8 is required for anterior heart field development.
1282 Development 133, 2435-2445.

bioRxiv preprint doi: https://doi.org/10.1101/138701; this version posted January 12, 2018. The copyright holder for this preprint (which was not certified by peer review) is the author/funder. All rights reserved. No reuse allowed without permission.

1283 Imai, K.S., Levine, M., Satoh, N., Satou, Y., 2006. Regulatory blueprint for a chordate
1284 embryo. Science 312, 1183-1187.

1285 Imai, K.S., Satoh, N., Satou, Y., 2002. Early embryonic expression of FGF4/6/9 gene
1286 and its role in the induction of mesenchyme and notochord in Ciona savignyi embryos.
1287 Development 129, 1729-1738.

1288 Jeffery, W.R., Chiba, T., Krajka, F.R., Deyts, C., Satoh, N., Joly, J.S., 2008. Trunk
1289 lateral cells are neural crest-like cells in the ascidian Ciona intestinalis: insights into the
1290 ancestry and evolution of the neural crest. Developmental biology 324, 152-160.

1291 Jerome, L.A., Papaioannou, V.E., 2001. DiGeorge syndrome phenotype in mice
1292 mutant for the T-box gene, Tbx1. Nature genetics 27, 286-291.

1293 Kaplan, N., Razy-Krajka, F., Christiaen, L., 2015. Regulation and evolution of
1294 cardiopharyngeal cell identity and behavior: insights from simple chordates. Current
1295 opinion in genetics & development 32, 119-128.

1296 Kattman, S.J., Witty, A.D., Gagliardi, M., Dubois, N.C., Niapour, M., Hotta, A., Ellis,
1297 J., Keller, G., 2011. Stage-specific optimization of activin/nodal and BMP signaling
1298 promotes cardiac differentiation of mouse and human pluripotent stem cell lines. Cell
1299 stem cell 8, 228-240.

1300 Keduka, E., Kaiho, A., Hamada, M., Watanabe-Takano, H., Takano, K., Ogasawara,
1301 M., Satou, Y., Satoh, N., Endo, T., 2009. M-Ras evolved independently of R-Ras and its
1302 neural function is conserved between mammalian and ascidian, which lacks classical
1303 Ras. Gene 429, 49-58.

1304 Kelly, R.G., Jerome-Majewska, L.A., Papaioannou, V.E., 2004. The del22q11.2
1305 candidate gene Tbx1 regulates branchiomeric myogenesis. Human molecular genetics
1306 13, 2829-2840.

1307 Kelly, R.G., Papaioannou, V.E., 2007. Visualization of outflow tract development in
1308 the absence of Tbx1 using an FgF10 enhancer trap transgene. Developmental dynamics :
1309 an official publication of the American Association of Anatomists 236, 821-828.

1310 Khan, A., Fornes, O., Stigliani, A., Gheorghe, M., Castro-Mondragon, J.A., van der
1311 Lee, R., Bessy, A., Cheneby, J., Kulkarni, S.R., Tan, G., Baranasic, D., Arenillas, D.J.,
1312 Sandelin, A., Vandepoele, K., Lenhard, B., Ballester, B., Wasserman, W.W., Parcy, F.,
1313 Mathelier, A., 2017. JASPAR 2018: update of the open-access database of transcription
1314 factor binding profiles and its web framework. Nucleic acids research.

1315 Khoueiry, P., Rothbacher, U., Ohtsuka, Y., Daian, F., Frangulian, E., Roure, A.,
1316 Dubchak, I., Lemaire, P., 2010. A cis-regulatory signature in ascidians and flies,
1317 independent of transcription factor binding sites. Current biology : CB 20, 792-802.

1318 Kuwajima, M., Kumano, G., Nishida, H., 2014. Regulation of the number of cell
1319 division rounds by tissue-specific transcription factors and Cdk inhibitor during
1320 ascidian embryogenesis. PloS one 9, e90188.

bioRxiv preprint doi: https://doi.org/10.1101/138701; this version posted January 12, 2018. The copyright holder for this preprint (which was not certified by peer review) is the author/funder. All rights reserved. No reuse allowed without permission.

Lazic, S., Scott, I.C., 2011. Mef2cb regulates late myocardial cell addition from a second heart field-like population of progenitors in zebrafish. Developmental biology 354, 123-133.

Lemmon, M.A., Schlessinger, J., 2010. Cell signaling by receptor tyrosine kinases. Cell 141, 1117-1134.

Lescroart, F., Chabab, S., Lin, X., Rulands, S., Paulissen, C., Rodolosse, A., Auer, H., Achouri, Y., Dubois, C., Bondue, A., Simons, B.D., Blanpain, C., 2014. Early lineage restriction in temporally distinct populations of Mesp1 progenitors during mammalian heart development. Nature cell biology 16, 829-840.

Lescroart, F., Hamou, W., Francou, A., Theveniau-Ruissy, M., Kelly, R.G., Buckingham, M., 2015. Clonal analysis reveals a common origin between nonsomite-derived neck muscles and heart myocardium. Proceedings of the National Academy of Sciences of the United States of America 112, 1446-1451.

Lescroart, F., Kelly, R.G., Le Garrec, J.F., Nicolas, J.F., Meilhac, S.M., Buckingham, M., 2010. Clonal analysis reveals common lineage relationships between head muscles and second heart field derivatives in the mouse embryo. Development 137, 3269-3279.

Lescroart, F., Mohun, T., Meilhac, S.M., Bennett, M., Buckingham, M., 2012. Lineage tree for the venous pole of the heart: clonal analysis clarifies controversial genealogy based on genetic tracing. Circulation research 111, 1313-1322.

Mandal, A., Holowiecki, A., Song, Y.C., Waxman, J.S., 2017. Wnt signaling balances specification of the cardiac and pharyngeal muscle fields. Mechanisms of Development 143, 32-41.

Mansour, S.J., Resing, K.A., Candi, J.M., Hermann, A.S., Gloor, J.W., Herskind, K.R., Wartmann, M., Davis, R.J., Ahn, N.G., 1994. Mitogen-activated protein (MAP) kinase phosphorylation of MAP kinase kinase: determination of phosphorylation sites by mass spectrometry and site-directed mutagenesis. Journal of biochemistry 116, 304-314.

Marques, S.R., Lee, Y., Poss, K.D., Yelon, D., 2008. Reiterative roles for FGF signaling in the establishment of size and proportion of the zebrafish heart. Developmental biology 321, 397-406.

Mazzoni, E.O., Mahony, S., Iacovino, M., Morrison, C.A., Mountoufaris, G., Closser, M., Whyte, W.A., Young, R.A., Kyba, M., Gifford, D.K., Wichterle, H., 2011. Embryonic stem cell-based mapping of developmental transcriptional programs. Nature methods 8, 1056-1058.

Merscher, S., Funke, B., Epstein, J.A., Heyer, J., Puech, A., Lu, M.M., Xavier, R.J., Demay, M.B., Russell, R.G., Factor, S., Tokooya, K., Jore, B.S., Lopez, M., Pandita, R.K., Lia, M., Carrion, D., Xu, H., Schorle, H., Kobler, J.B., Scambler, P., Wynshaw-Boris, A., Skoultchi, A.I., Morrow, B.E., Kucherlapati, R., 2001. TBX1 is responsible for cardiovascular defects in velo-cardio-facial/DiGeorge syndrome. Cell 104, 619-629.

Michailovici, I., Eigler, T., Tzahor, E., 2015. Craniofacial Muscle Development. Current topics in developmental biology 115, 3-30.

bioRxiv preprint doi: https://doi.org/10.1101/138701; this version posted January 12, 2018. The copyright holder for this preprint (which was not certified by peer review) is the author/funder. All rights reserved. No reuse allowed without permission.

Michailovici, I., Harrington, H.A., Azogui, H.H., Yahalom-Ronen, Y., Plotnikov, A., Ching, S., Stumpf, M.P., Klein, O.D., Seger, R., Tzahor, E., 2014. Nuclear to cytoplasmic shuttling of ERK promotes differentiation of muscle stem/progenitor cells. Development 141, 2611-2620.

Mosimann, C., Panakova, D., Werdich, A.A., Musso, G., Burger, A., Lawson, K.L., Carr, L.A., Nevis, K.R., Sabeh, M.K., Zhou, Y., Davidson, A.J., DiBiase, A., Burns, C.E., Burns, C.G., MacRae, C.A., Zon, L.I., 2015. Chamber identity programs drive early functional partitioning of the heart. Nature communications 6, 8146.

Nathan, E., Monovich, A., Tirosh-Finkel, L., Harrelson, Z., Rousso, T., Rinon, A., Harel, I., Evans, S.M., Tzahor, E., 2008. The contribution of Islet1-expressing splanchnic mesoderm cells to distinct branchiomeric muscles reveals significant heterogeneity in head muscle development. Development 135, 647-657.

Nevis, K., Obregon, P., Walsh, C., Guner-Ataman, B., Burns, C.G., Burns, C.E., 2013. Tbx1 is required for second heart field proliferation in zebrafish. Developmental dynamics : an official publication of the American Association of Anatomists 242, 550-559.

Norton, J., Cooley, J., Islam, A.F., Cota, C.D., Davidson, B., 2013. Matrix adhesion polarizes heart progenitor induction in the invertebrate chordate Ciona intestinalis. Development 140, 1301-1311.

Park, E.J., Ogden, L.A., Talbot, A., Evans, S., Cai, C.L., Black, B.L., Frank, D.U., Moon, A.M., 2006. Required, tissue-specific roles for Fgf8 in outflow tract formation and remodeling. Development 133, 2419-2433.

Park, E.J., Watanabe, Y., Smyth, G., Miyagawa-Tomita, S., Meyers, E., Klingensmith, J., Camenisch, T., Buckingham, M., Moon, A.M., 2008. An FGF autocrine loop initiated in second heart field mesoderm regulates morphogenesis at the arterial pole of the heart. Development 135, 3599-3610.

Patterson, K.I., Brummer, T., O'Brien, P.M., Daly, R.J., 2009. Dual-specificity phosphatases: critical regulators with diverse cellular targets. The Biochemical journal 418, 475-489.

Pauklin, S., Madrigal, P., Bertero, A., Vallier, L., 2016. Initiation of stem cell differentiation involves cell cycle-dependent regulation of developmental genes by Cyclin D. Genes & development 30, 421-433.

Pauklin, S., Vallier, L., 2013. The cell-cycle state of stem cells determines cell fate propensity. Cell 155, 135-147.

Peljto, M., Wichterle, H., 2011. Programming embryonic stem cells to neuronal subtypes. Current opinion in neurobiology 21, 43-51.

Pennati, R., Ficetola, G.F., Brunetti, R., Caicci, F., Gasparini, F., Griggio, F., Sato, A., Stach, T., Kaul-Strehlow, S., Gissi, C., Manni, L., 2015. Morphological Differences between Larvae of the Ciona intestinalis Species Complex: Hints for a Valid Taxonomic Definition of Distinct Species. PloS one 10, e0122879.

bioRxiv preprint doi: https://doi.org/10.1101/138701; this version posted January 12, 2018. The copyright holder for this preprint (which was not certified by peer review) is the author/funder. All rights reserved. No reuse allowed without permission.

1402 Picco, V., Hudson, C., Yasuo, H., 2007. Ephrin-Eph signalling drives the asymmetric
1403 division of notochord/neural precursors in Ciona embryos. Development 134, 1491-
1404 1497.

1405 Prall, O.W., Menon, M.K., Solloway, M.J., Watanabe, Y., Zaffran, S., Bajolle, F.,
1406 Biben, C., McBride, J.J., Robertson, B.R., Chaulet, H., Stennard, F.A., Wise, N., Schaft,
1407 D., Wolstein, O., Furtado, M.B., Shiratori, H., Chien, K.R., Hamada, H., Black, B.L.,
1408 Saga, Y., Robertson, E.J., Buckingham, M.E., Harvey, R.P., 2007. An Nkx2-
1409 5/Bmp2/Smad1 negative feedback loop controls heart progenitor specification and
1410 proliferation. Cell 128, 947-959.

1411 Putnam, N.H., Butts, T., Ferrier, D.E., Furlong, R.F., Hellsten, U., Kawashima, T.,
1412 Robinson-Rechavi, M., Shoguchi, E., Terry, A., Yu, J.K., Benito-Gutierrez, E.L.,
1413 Dubchak, I., Garcia-Fernandez, J., Gibson-Brown, J.J., Grigoriev, I.V., Horton, A.C., de
1414 Jong, P.J., Jurka, J., Kapitonov, V.V., Kohara, Y., Kuroki, Y., Lindquist, E., Lucas, S.,
1415 Osoegawa, K., Pennacchio, L.A., Salamov, A.A., Satou, Y., Sauka-Spengler, T., Schmutz,
1416 J., Shin, I.T., Toyoda, A., Bronner-Fraser, M., Fujiyama, A., Holland, L.Z., Holland,
1417 P.W., Satoh, N., Rokhsar, D.S., 2008. The amphioxus genome and the evolution of the
1418 chordate karyotype. Nature 453, 1064-1071.

1419 Racioppi, C., Kamal, A.K., Razy-Krajka, F., Gambardella, G., Zanetti, L., di Bernardo,
1420 D., Sanges, R., Christiaen, L.A., Ristoratore, F., 2014. Fibroblast growth factor signalling
1421 controls nervous system patterning and pigment cell formation in Ciona intestinalis.
1422 Nature communications 5, 4830.

1423 Razy-Krajka, F., Lam, K., Wang, W., Stolfi, A., Joly, M., Bonneau, R., Christiaen, L.,
1424 2014. Collier/OLF/EBF-Dependent Transcriptional Dynamics Control Pharyngeal
1425 Muscle Specification from Primed Cardiopharyngeal Progenitors. Developmental cell
1426 29, 263-276.

1427 Reifers, F., Walsh, E.C., Leger, S., Stainier, D.Y., Brand, M., 2000. Induction and
1428 differentiation of the zebrafish heart requires fibroblast growth factor 8
1429 (fgf8/acerebellar). Development 127, 225-235.

1430 Satou, Y., Imai, K.S., Satoh, N., 2004. The ascidian Mesp gene specifies heart
1431 precursor cells. Development 131, 2533-2541.

1432 Shi, W., Levine, M., 2008. Ephrin signaling establishes asymmetric cell fates in an
1433 endomesoderm lineage of the Ciona embryo. Development 135, 931-940.

1434 Shi, W., Peyrot, S.M., Munro, E., Levine, M., 2009. FGF3 in the floor plate directs
1435 notochord convergent extension in the Ciona tadpole. Development 136, 23-28.

1436 Soufi, A., Dalton, S., 2016. Cycling through developmental decisions: how cell cycle
1437 dynamics control pluripotency, differentiation and reprogramming. Development 143,
1438 4301-4311.

1439 Stolfi, A., Gainous, T.B., Young, J.J., Mori, A., Levine, M., Christiaen, L., 2010. Early
1440 chordate origins of the vertebrate second heart field. Science 329, 565-568.

1441 Stolfi, A., Gandhi, S., Salek, F., Christiaen, L., 2014a. Tissue-specific genome editing
1442 in Ciona embryos by CRISPR/Cas9. Development 141, 4115-4120.

bioRxiv preprint doi: https://doi.org/10.1101/138701; this version posted January 12, 2018. The copyright holder for this preprint (which was not certified by peer review) is the author/funder. All rights reserved. No reuse allowed without permission.

1443 Stolfi, A., Lowe, E.K., Racioppi, C., Ristoratore, F., Brown, C.T., Swalla, B.J.,
1444 Christiaen, L., 2014b. Divergent mechanisms regulate conserved cardiopharyngeal
1445 development and gene expression in distantly related ascidians. eLife 3, e03728.

1446 Stolfi, A., Sasakura, Y., Satou, Y., Christiaen, L., Dantec, C., Endo, T., Naville, M.,
1447 Nishida, H., Swalla, B., Volff, J.-N., Voskoboynik, A., Dauga, D., Lemaire, P., 2014c.
1448 Guidelines for the Nomenclature of Genetic Elements in Tunicate Genomes. Genesis
1449 under review.

1450 Stolfi, A., Wagner, E., Taliaferro, J.M., Chou, S., Levine, M., 2011. Neural tube
1451 patterning by Ephrin, FGF and Notch signaling relays. Development 138, 5429-5439.

1452 Tirosh-Finkel, L., Elhanany, H., Rinon, A., Tzahor, E., 2006. Mesoderm progenitor
1453 cells of common origin contribute to the head musculature and the cardiac outflow
1454 tract. Development 133, 1943-1953.

1455 Tirosh-Finkel, L., Zeisel, A., Brodt-Ivenshitz, M., Shamai, A., Yao, Z., Seger, R.,
1456 Domany, E., Tzahor, E., 2010. BMP-mediated inhibition of FGF signaling promotes
1457 cardiomyocyte differentiation of anterior heart field progenitors. Development 137,
1458 2989-3000.

1459 Tolkin, T., Christiaen, L., 2016. Rewiring of an ancestral Tbx1/10-Ebf-Mrf network
1460 for pharyngeal muscle specification in distinct embryonic lineages. Development in
1461 press.

1462 Tzahor, E., 2009. Heart and craniofacial muscle development: a new developmental
1463 theme of distinct myogenic fields. Developmental biology 327, 273-279.

1464 Tzahor, E., Evans, S.M., 2011. Pharyngeal mesoderm development during
1465 embryogenesis: implications for both heart and head myogenesis. Cardiovascular
1466 research 91, 196-202.

1467 Tzahor, E., Kempf, H., Mootoosamy, R.C., Poon, A.C., Abzhanov, A., Tabin, C.J.,
1468 Dietrich, S., Lassar, A.B., 2003. Antagonists of Wnt and BMP signaling promote the
1469 formation of vertebrate head muscle. Genes & development 17, 3087-3099.

1470 Tzahor, E., Lassar, A.B., 2001. Wnt signals from the neural tube block ectopic
1471 cardiogenesis. Genes & development 15, 255-260.

1472 van Wijk, B., van den Berg, G., Abu-Issa, R., Barnett, P., van der Velden, S., Schmidt,
1473 M., Ruijter, J.M., Kirby, M.L., Moorman, A.F., van den Hoff, M.J., 2009. Epicardium
1474 and myocardium separate from a common precursor pool by crosstalk between bone
1475 morphogenetic protein- and fibroblast growth factor-signaling pathways. Circulation
1476 research 105, 431-441.

1477 Vitelli, F., Morishima, M., Taddei, I., Lindsay, E.A., Baldini, A., 2002a. Tbx1
1478 mutation causes multiple cardiovascular defects and disrupts neural crest and cranial
1479 nerve migratory pathways. Human molecular genetics 11, 915-922.

1480 Vitelli, F., Taddei, I., Morishima, M., Meyers, E.N., Lindsay, E.A., Baldini, A., 2002b.
1481 A genetic link between Tbx1 and fibroblast growth factor signaling. Development 129,
1482 4605-4611.

bioRxiv preprint doi: https://doi.org/10.1101/138701; this version posted January 12, 2018. The copyright holder for this preprint (which was not certified by peer review) is the author/funder. All rights reserved. No reuse allowed without permission.

1483 von Scheven, G., Alvares, L.E., Mootoosamy, R.C., Dietrich, S., 2006. Neural tube
1484 derived signals and Fgf8 act antagonistically to specify eye versus mandibular arch
1485 muscles. Development 133, 2731-2745.

1486 Wagner, E., Stolfi, A., Gi Choi, Y., Levine, M., 2014. Islet is a key determinant of
1487 ascidian palp morphogenesis. Development 141, 3084-3092.

1488 Wang, W., Razy-Krajka, F., Siu, E., Ketcham, A., Christiaen, L., 2013. NK4
1489 antagonizes Tbx1/10 to promote cardiac versus pharyngeal muscle fate in the ascidian
1490 second heart field. PLoS biology 11, e1001725.

1491 Wang, W., Xiang, S., Jullian, E., Kelly, R.G., Satija, R., Christiaen, L., 2017. A single
1492 cell transcriptional roadmap for cardiopharyngeal fate diversification. BioRxiv.

1493 Watanabe, Y., Miyagawa-Tomita, S., Vincent, S.D., Kelly, R.G., Moon, A.M.,
1494 Buckingham, M.E., 2010. Role of mesodermal FGF8 and FGF10 overlaps in the
1495 development of the arterial pole of the heart and pharyngeal arch arteries. Circulation
1496 research 106, 495-503.

1497 Watanabe, Y., Zaffran, S., Kuroiwa, A., Higuchi, H., Ogura, T., Harvey, R.P., Kelly,
1498 R.G., Buckingham, M., 2012. Fibroblast growth factor 10 gene regulation in the second
1499 heart field by Tbx1, Nkx2-5, and Islet1 reveals a genetic switch for down-regulation in
1500 the myocardium. Proceedings of the National Academy of Sciences of the United States
1501 of America 109, 18273-18280.

1502 Weirauch, M.T., Yang, A., Albu, M., Cote, A.G., Montenegro-Montero, A., Drewe, P.,
1503 Najafabadi, H.S., Lambert, S.A., Mann, I., Cook, K., Zheng, H., Goity, A., van Bakel, H.,
1504 Lozano, J.C., Galli, M., Lewsey, M.G., Huang, E., Mukherjee, T., Chen, X., Reece-Hoyes,
1505 J.S., Govindarajan, S., Shaulsky, G., Walhout, A.J.M., Bouget, F.Y., Ratsch, G.,
1506 Larrondo, L.F., Ecker, J.R., Hughes, T.R., 2014. Determination and inference of
1507 eukaryotic transcription factor sequence specificity. Cell 158, 1431-1443.

1508 Whittaker, J.R., 1973. Segregation during ascidian embryogenesis of egg cytoplasmic
1509 information for tissue-specific enzyme development. Proceedings of the National
1510 Academy of Sciences of the United States of America 70, 2096-2100.

1511 Witzel, H.R., Cheedipudi, S., Gao, R., Stainier, D.Y., Dobreva, G.D., 2017. Isl2b
1512 regulates anterior second heart field development in zebrafish. Scientific reports 7,
1513 41043.

1514 Woznica, A., Haeussler, M., Starobinska, E., Jemmett, J., Li, Y., Mount, D.,
1515 Davidson, B., 2012. Initial deployment of the cardiogenic gene regulatory network in the
1516 basal chordate, Ciona intestinalis. Developmental biology 368, 127-139.

1517 Yagi, H., Furutani, Y., Hamada, H., Sasaki, T., Asakawa, S., Minoshima, S., Ichida, F.,
1518 Joo, K., Kimura, M., Imamura, S., Kamatani, N., Momma, K., Takao, A., Nakazawa, M.,
1519 Shimizu, N., Matsuoka, R., 2003. Role of TBX1 in human del22q11.2 syndrome. Lancet
1520 362, 1366-1373.

1521 Yasuo, H., Hudson, C., 2007. FGF8/17/18 functions together with FGF9/16/20
1522 during formation of the notochord in Ciona embryos. Developmental biology 302, 92-
1523 103.

bioRxiv preprint doi: https://doi.org/10.1101/138701; this version posted January 12, 2018. The copyright holder for this preprint (which was not certified by peer review) is the author/funder. All rights reserved. No reuse allowed without permission.

1524 Zaffran, S., Frasch, M., 2002. Early signals in cardiac development. Circulation
1525 research 91, 457-469.

1526 Zhang, Z., Huynh, T., Baldini, A., 2006. Mesodermal expression of Tbx1 is necessary
1527 and sufficient for pharyngeal arch and cardiac outflow tract development. Development
1528 133, 3587-3595.
1529